Boussinesq Modeling of Wave Transformation, Breaking and Runup

Part I: One Dimension

A. B. Kennedy, Q. Chen, J. T. Kirby and R. A. Dalrymple

Part II: Two Horizontal Dimensions

Q. Chen, J. T. Kirby, R. A. Dalrymple, A. B. Kennedy and Arun Chawla

RESEARCH REPORT NO. CACR-99-02
March, 1999

Center for Applied Coastal Research
Ocean Engineering Laboratory
University of Delaware
Newark, DE 19716

BOUSSINESQ MODELING OF WAVE TRANSFORMATION, BREAKING AND RUNUP. I: ONE DIMENSION[1]

A.B. Kennedy[2], Q. Chen[1], J.T. Kirby[1], and R.A. Dalrymple[1]

Abstract

Parts I and II of this paper describe the extension of the Boussinesq equations of Nwogu (1993) and Wei et al. (1995) to include surf zone phenomena. Part I is restricted to one dimensional tests of breaking and runup, while part II deals with two horizontal dimensions. The model uses two main extensions to the Boussinesq equations: a momentum conserving eddy viscosity technique to model breaking, and a "slotted beach", which simulates a shoreline while allowing computations over a regular domain. Bottom friction is included using a quadratic representation, while the two dimensional implementation of the model also considers subgrid mixing. Comparisons with experimental data show good agreement for a variety of wave conditions.

1 Introduction

It has long been a goal of coastal engineers to produce a computational wave model that is capable of simulating accurately wave motion from deep water through the surf zone. To do this, a model would have to include, among other things, nonlinear shoaling, refraction, diffraction, wave-wave interaction, breaking and runup. As it is currently impractical to perform a full solution of

[1]Submitted for *J. Waterway, Port Coastal and Ocean Engineering*

[2]Center for Applied Coastal Research, University of Delaware, Newark, DE 19716.

the Navier-Stokes equations over any significant domain, approximate models must be used.

One set of candidate models is the various Boussinesq-type equations (Peregrine, 1967; Madsen and Sørensen, 1992; Nwogu, 1993; Wei et al., 1995). These can describe, to varying degrees of accuracy in representing nonlinearity and dispersion, most phenomena exhibited by nonbreaking waves in finite depths. However, as derived they do not include dissipation due to wave breaking and thus become invalid in the surf zone. Accordingly, there have been attempts to introduce wave breaking into Boussinesq models. Heitner and Housner (1970) introduced artificial viscosity terms into momentum conservation equations in order to capture the shock across a tsunami bore. These terms conserved overall momentum, which is very important for a breaking scheme. Tao (1983,1984) used a crude nonconservative eddy viscosity term in order to model breaking. Zelt (1991) used an eddy viscosity formulation which was somewhat similar to that of Heitner and Housner together with a Lagrangian Boussinesq model to study the breaking and runup of solitary waves. However, in the conversion, the breaking term lost its momentum conserving form. Using a roller-based approximation, Schäffer et al., 1993, and Madsen et al., 1997a, (referred here as DHI) have developed a comprehensive breaking and surf zone model based on a flux version of the Boussinesq equations which can model breaking phenomena such as wave height decay, wave-induced setup, and runup. Svendsen et al. (1996) developed a breaking wave model that consistently includes rotational effects caused by breaking in order to model dissipation. They also compared their model with the DHI roller model, and a precursor to the model described here (Wei and Kirby, 1996), and found similarities in all three techniques.

This and a companion paper (Chen et al., 1999) document the extension of the fully nonlinear Boussinesq equations of Wei et al. (1995) and the extended

Boussinesq equations of Nwogu (1993) to include surf zone phenomena related to wave breaking and runup. In this paper, the surf zone model is introduced and its performance for one dimensional breaking and runup is examined. Part II (Chen et al., 1999) considers surf zone modelling for two horizontal dimensions. An additional, related, paper considers the Boussinesq modelling of a rip current system (Chen et al., 1998).

The basis of the breaking scheme used here is a simple eddy viscosity-type model, in contrast to some of the more complicated techniques available. This is somewhat like the eddy viscosity formulation of Heitner and Housner (1970) or Zelt (1991), but with extensions to provide a more realistic description of the initiation and cessation of wave breaking. Comparisons are made with laboratory results for one dimensional breaking and shoreline runup, with generally good results. The shoreline is treated using an improved version of the slot method described by Tao (1983, 1984).

2 The Surf Zone Model

2.1 Breaking Model

Both the extended Boussinesq equations of Nwogu (1993) and Wei et al. (1995, WKGS) are written in terms of a reference velocity $\mathbf{u}_\alpha = (u_\alpha, v_\alpha)$ at some reference elevation z_α. The WKGS equation for conservation of mass may be written as

$$\eta_t + \nabla \cdot \mathbf{M} = 0 \tag{1}$$

where h is the still water depth, η is the free surface elevation and

$$\mathbf{M} = (h+\eta)\left[\mathbf{u}_\alpha + \left(\frac{{z_\alpha}^2}{2} - \frac{1}{6}(h^2 - h\eta + \eta^2)\right)\nabla(\nabla \cdot \mathbf{u}_\alpha)\right.$$

$$+\left[z_\alpha+\frac{1}{2}(h-\eta)\right]\nabla\left(\nabla\cdot\left(h\mathbf{u}_\alpha\right)\right)\Big] \tag{2}$$

The associated momentum conservation equation is

$$\mathbf{u}_{\alpha t}+\left(\mathbf{u}_\alpha\cdot\nabla\right)\mathbf{u}_\alpha+g\nabla\eta+\mathbf{V}_1+\mathbf{V}_2=0 \tag{3}$$

where g is the downwards gravitational acceleration, and $\mathbf{V}_1$ and $\mathbf{V}_2$ are the dispersive Boussinesq terms

$$\mathbf{V}_1 = \frac{{z_\alpha}^2}{2}\nabla\left(\nabla\cdot\mathbf{u}_{\alpha t}\right)+z_\alpha\nabla\left(\nabla\cdot(h\mathbf{u}_{\alpha t})\right)-\nabla\left[\frac{\eta^2}{2}\nabla\cdot\mathbf{u}_{\alpha t}+\eta\nabla\cdot(h\mathbf{u}_{\alpha t})\right] \tag{4}$$

$$\begin{aligned}\mathbf{V}_2 = {} & \nabla\left[\left(z_\alpha-\eta\right)\left(\mathbf{u}_\alpha\cdot\nabla\right)\left(\nabla\cdot(h\mathbf{u}_\alpha)\right)+\frac{1}{2}({z_\alpha}^2-\eta^2)(\mathbf{u}_\alpha\cdot\nabla)(\nabla\cdot\mathbf{u}_\alpha)\right] \\ & +\frac{1}{2}\nabla\left[\left(\nabla\cdot(h\mathbf{u}_\alpha)+\eta\nabla\cdot\mathbf{u}_\alpha\right)^2\right]\end{aligned} \tag{5}$$

Nwogu's equations are recovered by neglecting nonlinear dispersive terms. The mass conservation equation remains in the form of (1), but with

$$\mathbf{M}=(h+\eta)\mathbf{u}_\alpha+(\frac{h{z_\alpha}^2}{2}-\frac{h^3}{6})\nabla(\nabla\cdot\mathbf{u}_\alpha)+(hz_\alpha+\frac{h^2}{2})\nabla\left(\nabla\cdot(h\mathbf{u}_\alpha)\right) \tag{6}$$

while the equation for momentum conservation becomes

$$\mathbf{u}_{\alpha t}+(\mathbf{u}_\alpha\cdot\nabla)\mathbf{u}_\alpha+g\nabla\eta+\frac{{z_\alpha}^2}{2}\nabla(\nabla\cdot\mathbf{u}_{\alpha t})+z_\alpha\nabla(\nabla\cdot(h\mathbf{u}_{\alpha t}))=0 \tag{7}$$

Linear dispersion properties vary with the choice of z_α. Nwogu (1993) describes an error-minimising condition which when applied to the range $0<kh<\pi$ yields the result $z_\alpha=-0.531h$, which will be used in all calculations.

The above equations are only valid for nonbreaking waves, so some additional approximation must be made to model wave breaking. In contrast to some of the more complicated methods mentioned earlier, a simple eddy viscosity-type formulation is used to model the turbulent mixing and dissipation caused by breaking. The mass conservation equation (1) remains unchanged, while, with the additional eddy viscosity terms, the equation for momentum conservation becomes

$$\mathbf{u}_{\alpha t}+\ldots-\mathbf{R_b}=0 \tag{8}$$

where

$$\mathbf{R_{bx}} = \frac{1}{h+\eta}\left([\nu((h+\eta)u_\alpha)_x]_x + \frac{1}{2}[\nu((h+\eta)u_\alpha)_y + \nu((h+\eta)v_\alpha)_x]_y\right) \quad (9)$$

$$\mathbf{R_{by}} = \frac{1}{h+\eta}\left([\nu((h+\eta)v_\alpha)_y]_y + \frac{1}{2}[\nu((h+\eta)u_\alpha)_y + \nu((h+\eta)v_\alpha)_x]_x\right) \quad (10)$$

By multiplying the momentum equations by $h+\eta$ and integrating over a breaking event, these additional terms may be shown to conserve overall momentum. The model behaviour is thus consistent (in the region of a breaking wave crest) with the momentum-conserving bore process in open-channel flow.

The eddy viscosity, ν, which is a function of both space and time, is determined in a similar manner to Zelt (1991), but with several differences. The eddy viscosity is given here by

$$\nu = B\delta_b^2(h+\eta)\eta_t \quad (11)$$

where δ_b is a mixing length coefficient. From the results of many tests, it is set here to a dimensionless value of $\delta_b = 1.2$. Surprisingly, computations are relatively insensitive to changes in this parameter. The quantity B varies smoothly from 0 to 1 so as to avoid an impulsive start of breaking and the resulting instability. It is given by

$$B = \begin{cases} 1, & \eta_t \geq 2\eta_t^* \\ \frac{\eta_t}{\eta_t^*} - 1, & \eta_t^* < \eta_t \leq 2\eta_t^* \\ 0, & \eta_t \leq \eta_t^* \end{cases} \quad (12)$$

The parameter η_t^* determines the onset and the cessation of breaking. Use of η_t as an initiation parameter ensures in a simple manner that the dissipation is concentrated on the front face of the wave, as in nature. Zelt (1991) assumed that parameters of this sort would have a constant value, but this is not in accordance with reality. For example, in nature, spilling and plunging ocean waves do not begin to break until the wave overturns, but, once the wave has

broken, it will continue to break until it either reaches the beach, or arrives at some smaller stable level at which it will reform (e.g. Horikawa and Kuo, 1966). A similar assumption was used in the breaking model of Schäffer et al. (1993). In the present model, a breaking event begins when η_t exceeds some initial value but, as breaking develops, the wave will continue to break even if η_t drops below this value. The magnitude of η_t^* therefore decreases in time from some initial value $\eta_t^{(I)}$ to a terminal quantity $\eta_t^{(F)}$. No strong evidence exists for what form this decrease would take, so a simple linear relation is used here to model the evolution of η^*. This becomes

$$\eta_t^* = \begin{cases} \eta_t^{(F)}, & t \geq T^* \\ \eta_t^{(I)} + \frac{t-t_0}{T^*}(\eta_t^{(F)} - \eta_t^{(I)}), & 0 \leq t - t_0 < T^* \end{cases} \tag{13}$$

where T^* is the transition time, t_0 is the time that breaking was initiated, and thus $t - t_0$ is the age of the breaking event, which is non-negative. The default values of $\eta_t^{(I)}$ and $\eta_t^{(F)}$ used here are $0.65\sqrt{gh}$ and $0.15\sqrt{gh}$, respectively. The default transition time used here is $T^* = 5\sqrt{h/g}$. None of these quantities may be regarded as universal values; they were chosen on the basis of multiple tests with different parameter values to give good agreement with experimental measurements for the WKGS and Nwogu equations. For use in other Boussinesq models with different linear and nonlinear performance, care must be taken to ensure that these parameters are appropriate.

For wave motion in one horizontal dimension, breaking events are well defined. The quantity t_0, the time when breaking was initiated, will in general vary for different breaking events within a system, but it is a simple matter to track any particular event as it progresses towards the shore, and thus to know the age of each event. For example, in the outer surf zone a wave may have begun breaking a short time before the present. The age of breaking $t - t_0$ will thus be small and η_t^* will be slightly less than $\eta_t^{(I)}$. However, at the same time

there may be another breaking event in the inner surf zone where $t - t_0 > T^*$ and thus $\eta_t^* = \eta_t^{(F)}$.

For all breaking events, the eddy viscosity, ν, is filtered for stability using a three point filter before it is inserted into (9-10).

For two horizontal dimensions, the problem becomes slightly more difficult and is detailed in Part II by Chen et al. (1999).

2.2 Moving Shoreline

For computations of wave runup, and for computing wave motion over natural coasts, it is necessary for a wave model to be able to simulate the land-sea interface realistically. To do this, a modification of the slot method of Tao (1983, 1984) is used. In this, the entire computational domain is considered active, but where there is very little or no water covering the land, modified equations are solved. These equations assume that, instead of being solid, the beach is porous, or contains narrow "slots", so it is possible for the water level to be below the beach elevation. Alternatively, this method may be thought of as a "thin film" technique with a changed gravitational term, in which a very thin layer of water covers "dry" areas.

Madsen et al. (1997a-b) utilized a variant of the slot technique in an extended Boussinesq model formulated in terms of volume flux and free surface elevation, and demonstrated the effectiveness of the slot method for simulation of wave runup on beaches. Although the agreement between the modelled and measured swash motions on sloping fixed beds at laboratory scales was shown to be reasonably good by Madsen et al. (1997a), a comparison with the analytical solution of wave runup on a solid slope (Carrier and Greenspan, 1958) indicated that the slot method tended to underpredict the maximum runup

height with about a ten percent error even when a very narrow slot width was used. This was because, before water could cover a previously dry area, the slot first needed to be filled, decreasing slightly the overall volume available for runup. Because the maximum runup height is very sensitive to the total volume at the runup tip, runup is underpredicted. Thus, a slightly different formulation is proposed, which ensures that when the water level is above the top of the slot, there will be no net fluid loss at that location. Some small mass loss still exists from water flowing into the slots where the water level is below the top of the slot, but it is much reduced.

Figure 1 shows a schematic of a wave flume with a sloping bottom in the presence of a narrow slot. The width of the wave flume is defined as

$$b(\eta) = \begin{cases} 1, & \eta \geq z^* \\ \delta + (1-\delta)e^{\frac{\lambda(\eta - z^*)}{h_0}}, & \eta \leq z^* \end{cases} \tag{14}$$

in which δ is the slot width relative to a unit width of beach; λ is the shape parameter that controls the smooth transition of the cross-sectional area from a unit width to a narrow slot; z^* denotes the elevation of the seabed where $b = 1$; h_0 is a reference water depth that must be deeper than the water depth at the lower limit of the swash zone; and η is the free surface elevation relative to the still water level. Thus the cross-sectional area of the channel can be expressed by

$$A(\eta) = \begin{cases} (\eta - z^*) + \delta(z^* + h_0) + \frac{(1-\delta)h_0}{\lambda}(1 - e^{-\lambda(1+\frac{z^*}{h_0})}), & \eta \geq z^* \\ \delta(\eta + h_0) + \frac{(1-\delta)h_0}{\lambda}e^{\frac{\lambda(\eta - z^*)}{h_0}}(1 - e^{-\lambda(1+\frac{\eta}{h_0})}), & \eta \leq z^* \end{cases} \tag{15}$$

The equation for conservation of mass in the wave channel is:

$$A_t + (AU)_x = 0 \tag{16}$$

where U is the depth-averaged velocity. Omitting the effect of a narrow slot on the vertical distribution of the fluid particle velocity in the wave flume leads to

the mass equation formulated in terms of the velocity at the reference level z_α as follows

$$\beta\eta_t + M_x = 0 \tag{17}$$

in which

$$\begin{aligned} M &= \Lambda\left[u_\alpha + \left(\frac{{z_\alpha}^2}{2} - \frac{1}{6}(h^2 - h\eta + \eta^2)\right) u_{\alpha xx}\right. \\ &\quad \left. + \left(z_\alpha + \frac{1}{2}(h-\eta)\right)(hu_\alpha)_{xx}\right] \end{aligned} \tag{18}$$

Here $\beta = b(\eta)$ and $\Lambda = A(\eta)$. Equation (17) with (18) will replace the one-dimensional version of (1) and (2) for the simulation of wave runup using the slot technique. Since the presence of a narrow slot does not alter the momentum equations formulated in terms of velocity and surface elevation, the extension of this treatment of a moving shoreline to the case of two horizontal dimensions is straightforward. For detailed 2D applications, the reader is referred to Part II (Chen et al., 1999).

The fulfillment of mass conservation in the presence of an artificial slot depends on the choice of z^* in the functions β and Λ. In Tao's (1984) and Madsen et al.'s (1997a) formulation, z^* is chosen to be $z = -h$, the elevation of the physical solid seabed. This leads to an effective loss of mass during runup, as water must first fill the slots before it can wet the dry beach face. The opposite phenomenon occurs during rundown. Here, we choose z^* by specifying that, once the water level is above the the top of the slot, the overall volume will be identical to that if no slot existed. For $\eta \geq z^*$, equating the cross-sectional area with and without a slot leads to

$$\eta - z^* + \delta(z^* + h_0) + \frac{(1-\delta)h_0}{\lambda}(1 - e^{-\lambda(1+\frac{z^*}{h_0})}) = \eta - z \tag{19}$$

Using a Taylor expansion of $e^{\lambda\frac{(z^*-z)}{h_0}}$ around zero, and neglecting the second

order and higher terms, we obtain

$$z^* = \frac{z + \delta h_0}{(1-\delta)(1 - e^{-\lambda(1+\frac{z}{h_0})})} + \frac{h_0}{\lambda} \tag{20}$$

Since $\lambda \gg 1$ as used in practice, (20) can be simplified as

$$z^* = \frac{z}{1-\delta} + h_0(\frac{\delta}{1-\delta} + \frac{1}{\lambda}) \tag{21}$$

The choice of z^* as defined in (20) or (21) will lead to the improvement in the prediction of maximum runup height as shown in the following section where we shall discuss the optimal values of δ and λ.

3 Model Verification

3.1 Wave Breaking

To test performance of the breaking model, results were compared to regular and irregular wave breaking experiments. Comparisons began with a series of one dimensional regular wave tests on plane slopes. Five tests were chosen out of a large series performed by Hansen and Svendsen (1979), for conditions ranging from spilling to plunging breakers. Here, both experimental and computational wave generators added a second harmonic to the input signals, with amplitude and phase empirically chosen to minimise free second harmonics. Next, run 2 of the irregular wave tests of Mase and Kirby (1992) was simulated. In addition to wave heights, time series of surface elevation and a wide range of statistical parameters were compared for these tests. For both sets of tests, the breaking parameters were set to the values given in section 2.1, and slot values were set to $\lambda = 80$ and $\delta = 0.005$.

3.1.1 Regular Waves

Hansen and Svendsen (1979) reported on a large series of shoaling and breaking tests involving regular waves. Waves were generated on a horizontal bottom at a depth of 0.36 m, shoaled, and broke on a 1:34.26 planar slope. Measurements of surface elevation were taken at a very large number of locations using an automated, continuously moving trolley. For the purposes of the present study, computed wave heights and setups were compared with the measured values both seaward of and inside the surf zone.

Because of the moving trolley used in the experiment and the correspondingly small sample size at any particular location, measurements showed considerable scatter, especially in the surf zone. For this study, they were therefore smoothed somewhat by averaging the results at any three adjacent measurement locations, and rounding to the nearest mm for wave heights and 0.1 mm for setup. Since the measurement locations were typically separated by only a few cm, the evolution of a wave between adjacent locations was usually insignificant, while the averaging process reduced scatter considerably. Even with this reduction of data, there were still hundreds of measurements for each wave condition, so the data set was further reduced to approximately 40-45 per wave, which gave a good description of the wave shoaling and breaking. Further, Hansen and Svendsen's estimates of overall water volume showed that "a certain amount of water seems to be pumped to the inactive part of the flume behind the sloping bottom during the test". This resulted in a decrease in mean water level over the active part of the flume. To compensate for this loss of water, and because the experimental and computational wave tanks had different total volumes, small offsets were applied here to some of the experimental runs to match computed values of setdown in the deeper part of the

tank.

Five cases were simulated here, covering a wide range of breaker types, and serving as an necessary initial test for the surf zone model. Table 1 lists characteristics for all waves tested. Breaker types are based on a surf similarity analysis, initial wavenumbers are computed from linear theory, and wavenumbers at breaking are taken from Hansen and Svendsen (1979).

Case	T(s)	H_0(cm)	Breaker type	$kh_{(I)}$	$kh_{(Br)}$
031041	3.33	4.3	plunging	0.369	0.18
041041	2.5	3.9	spilling-plunging	0.501	0.24
051041	2.0	3.6	spilling	0.641	0.27
061071	1.67	6.7	spilling	0.791	0.41
A10112	1.0	6.7	spilling	1.58	0.76

Table 1: Experimental wave parameters for Hansen and Svendsen tests.

The first test, case 031041 as defined in Table 1, was well into the plunging regime. Figure 2 shows computed and measured wave heights as the wave propagates up the slope. Heights using the WKGS and Nwogu equations are reasonable as the wave shoals and breaks. However, both sets of equations appear to slightly underpredict the peak wave height at breaking. The setup trend is predicted well. For this and many of the other waves tested, some backwards-propagating short wave noise was generated during breaking. This had the effect of increasing the measured crest-to-trough height, both in the surf zone and offshore. For this particular test, this meant that matching wave heights offshore may have led to an underestimate of the primary wave height, and the consequent undershoaling. This test also shows clearly one of

the two most significant sources of error. Although agreement is, on the whole, reasonable, wave heights in the inner surf zone are overpredicted, a trend which proved very robust to changes in the breaking parameters. It is unclear whether this result derives from the breaking model, the Boussinesq equations used, or some combination of the two.

The next breaker, case 041041, was somewhat shorter and was near the plunging-spilling transition. Figure 3 shows computed and measured wave evolution and setup. Once again, the WKGS equations give a good description of wave shoaling and breaking, although wave heights are slightly overpredicted as the wave shoals, and thus the computational wave breaks slightly early. Computations using Nwogu's equations show a similar trend, although the overshoaling is further exaggerated. Comparing setup, both sets of Boussinesq equations give good results, although setup begins slightly early, which follows directly from the error in the breakpoint location.

Figure 4 shows computed and measured wave heights for case 051041. This shows a similar trend to the previous case. Wave shoaling is again predicted moderately well, but with overshoaling. Wave induced setup for this case also appears reasonable, but a small difference in setdown slope may be discerned.

The observed overshoaling was seen to some degree in most tests and is believed to be a result of the tendency of the WKGS and Nwogu equations to overpredict the magnitude of nonlinear superharmonics somewhat in intermediate depths. For long waves, the WGKS equations provide very good predictions of solitary wave shoaling to near the breaking limit, while Nwogu's equations predict reasonable, though somewhat large, wave heights (Wei at al., 1995, Figures 4-5). However, for waves in intermediate depth, nonlinear errors increase for both sets of equations. Figure 5.3 in Madsen and Schäffer (1998) shows that for dimensionless wavenumbers of $kh < 1.5$, which is approximately

the range considered in these tests, Nwogu's equations show a maximum of about 20 per cent overprediction in the bound second harmonic of a second order steady wave. In contrast, the WGKS equations have maximum errors of around 10 per cent over this range. These bound second order harmonics can not cause overshoaling; however, errors in third harmonics, which generally follow the trend of second order solutions, will be noticed as overpredictions or underpredictions of computed wave heights. This is believed to be the cause of the observed overshoaling in some tests.

Figure 5 shows computed wave heights for case 061071, which was another spilling breaker, with period 1.67 s and height 6.7 cm. Again, the trends are all very similar to the previous cases, with overshoaling and somewhat premature breaking. Overall agreement for wave heights and setup appears to be comparable to the previous case. Once again, Nwogu's equations have a slightly worse prediction of setup than the WKGS equations shoreward of the break point.

The final wave tested from Hansen and Svendsen's tests was a spilling breaker with period 1.0 s and height 6.7 cm. This was designated case A10112. Figure 6 shows wave heights. Once again, overshoaling occurs, but agreement is better than the previous wave. No strong comparison may be made for setup in this case, as there is little data shoreward of the breakpoint. From the little available, computed setup using Nwogu's equations appears to increase somewhat more quickly after breaking than measured values.

Overall, although agreement is, on the whole, reasonable, some general error trends become clear. Wave heights in the inner surf zone are overpredicted, a trend which proved very robust to changes in the breaking parameters. It is unclear whether this result derives from the breaking model, the Boussinesq equations used, or some combination of the two.

3.1.2 Irregular Waves

For a test of model performance using irregular waves, the experiments of Mase and Kirby (1992) were simulated. Experiments were performed on a 1:20 planar slope using an incident Pierson-Moskowitz spectrum. Computational results were compared with data from Run 2, which had a peak frequency of 1.0 Hz and predominantly spilling breakers. Computations were initialised using a time series of data at the deepest measurement location denoted wave gage 1 in Figure 7, which was assumed to represent linear, unidirectional incident waves. A small offset was added to the experimental data to match computed values of setdown at the deepest measurement location.

Figure 8 shows a typical time series of computed and measured surface elevations at the other 11 wave gages using the WKGS equations. Agreement is in general quite good, but deteriorates as the waves progress towards shore. This was to be expected, as the assumption of linear, unreflected incident waves used to generate the waveforms could only be an approximation to reality.

Overall statistical parameters can provide a more detailed picture of the breaking model performance. Figure 9 shows standard deviations of measured and computed surface elevation, and wave setup. Agreement is reasonable, although, once again, wave heights near the shoreline become too large. Computed setup appears quite good, especially using the WKGS equations.

Wave asymmetry, a measure of left-right differences in a wave, and skewness, a measure of crest-trough shape, are computed from time series of surface elevation at chosen locations, and are shown in Figure 10. Asymmetry is defined as

$$As = \frac{\langle \mathcal{H}(\eta)^3 \rangle}{\langle \eta^2 \rangle^{3/2}} \tag{22}$$

where $\mathcal{H}$ denotes the Hilbert transform, $\langle\ \rangle$ is the mean operator, and the mean

has been removed from the time series of surface elevation. Skewness is defined as

$$Sk = \frac{\langle \eta^3 \rangle}{\langle \eta^2 \rangle^{3/2}} \tag{23}$$

using the zero mean surface elevation. Asymmetry is seen to increase steadily as the wave approaches the shoreline, corresponding to the well known steep front and gentle back slopes of highly nonlinear shoaling and breaking waves. Both sets of Boussinesq equations predict this parameter very well. The trend of wave skewness is also predicted well, increasing as the wave shoals and breaks, and then decreasing near the shoreline. Positive skewness here corresponds to narrow crests and flat troughs. Both sets of equations tend to slightly overpredict maximum skewness, likely because of the tendency towards overshoaling noted earlier.

3.2 Wave Runup

3.2.1 Non-breaking Long Waves

A standard test of a numerical scheme for shoreline runup is the solution of a nonlinear long wave on a sloping bottom. Carrier and Greenspan (1958) provided an analytical solution which was reproduced closely by Özkan-Haller and Kirby (1997) using a numerical model based on a Fourier-Chebyshev collocation method. We shall verify our numerical results against those computed by Özkan-Haller and Kirby's model.

For convenience of comparison, the test case of a non-breaking long wave on an impermeable slope as used by Madsen et al. (1997a) is repeated here. We consider a 10 s wave train with an initial wave height of 0.006 m in a wave channel containing a 1:25 slope. In the flat portion of the channel, the still water depth is 0.5 m. Wave runup and run-down on the slope result in a

standing wave form in the channel. Figure 11a-b shows the comparison of the spatial and temporal variations of the free surface and the horizontal shoreline motion computed by the present model with the slot technique and by Özkan-Haller and Kirby's (1997) model. The full lines represent the present results. We notice that the improved slot scheme as described in the preceding section predicts well the maximum runup height and surface depression as well as the standing wave form in comparison with the exact solution denoted by the dashed lines. A slight deviation is observed, however, in the antinodal free surface displacement between the first two nodes and the peak of the horizontal shoreline motion because of the approximate nature of the slot scheme. In this simulation, δ and λ are chosen to be 0.002 and 80, respectively. As suggested by Madsen et al. (1997a), a filter localized in the swash zone on the basis of a five-point weighted average is also used in order to suppress noise near the shoreline due to the use of the slot. We chose the grid size and time step to be 0.1 m and and 0.04 s, respectively. The Boussinesq terms are also switched off for consistency with the nonlinear shallow water equations.

The improvement in the prediction of maximum shoreline excursion by the corrected slot scheme retaining mass conservation is illustrated by Fig. 11c. In the figure, two curves respectively represent the computed maximum shoreline excursion as a function of the slot width taken relative to a unit width of beach by the use of the new and original definitions of z^*. We normalized the computed maximum shoreline excursion by the exact solution. The circles denote the numerical results of the present runup scheme with equivalent cross-sectional area while the stars are those using Tao's (1983) or Madsen et al.'s (1997a) scheme. Apparently, the proposed correction leads to much faster convergence in comparison with the results based on the original version of the slot technique. For example, with $\delta = 0.005$ and $\lambda = 80$, the improved slot scheme

predicts the maximum runup height with less than 5 percent error while the original one gives about 15 percent error in this test case.

3.2.2 Bichromatic waves

In a study of frequency downshift in the swash motion, Mase (1995) presented experimental results of bichromatic wave train runup on a slope. The experiments were conducted using the same wave flume and experimental setup as those in Mase and Kirby (1992) described in the preceding section. Mase's laboratory measurements, including shoaling, breaking and swash motion, provide good test cases for the verification of the runup scheme in combination with the wave breaking model.

We chose two typical test cases from Mase's (1995) series of experiments. Each of them represents a different kind of wave group pattern. The first one, named WP1, contains fives waves in each wave group with a mean frequency $f = 0.6$ Hz, while in the second case WP2, each wave group consists of ten waves with $f = 1.2$ Hz. In both cases, the nonlinear interactions of wave components and the variation of breaking point in the wave train, among others cause considerable low frequency swash oscillations. Unlike the simulation of Mase-Kirby's (1992) experiment, we use the Boussinesq model incorporating the improved slot scheme and the breaking model to simulate these two test cases.

Incident waves are generated using the source function technique developed by Wei et al. (1998). The measured time series of the free surface at Gauge 1 near the toe of the slope is used as an input to the model. As in the physical experiment, no effort is made to include bound second harmonics in the incident waves. Due to the presence of the slot inside the dry beach, the whole channel is an active computational domain with closed boundaries at each end of the wave

flume. To be able to resolve superharmonics in the wave train, the grid size and the time step is chosen to be 0.02 m and 0.01 s, respectively. With respect to the wave breaking model, the parameters are kept the same as those in the preceding simulations. For the slot scheme, we use $\delta = 0.005$, and $\lambda = 80$.

Comparisons of computed and measured surface elevation for the two test cases are presented in Figs. 12 and 13, including 11 wave gauges along the slope and a runup gauge. The dashed lines represent the computed results while the full lines are the measurements. Generally good agreement is found in both test cases.

First of all, we notice that the nonlinear shoaling of the bichromatic wave trains is well predicted by the Boussinesq model. Near the shoreline where wave breaking occur, although a slight discrepancy is observed, the overall agreement is satisfactory between the computed surface elevation and Mase's (1995) data. Moreover, the modelled swash motions are in good agreement with the measurements. The frequency downshift of the swash motion in comparison with the frequency of the incoming waves is well reproduced by the present model as illustrated in Fig. 14 where dashed lines denote the amplitude spectra offshore while solid lines are those in the swash zone. The good agreement demonstrates that the present Boussinesq model with the incorporation of the wave breaking model and the improved slot technique works reasonably well for the simulation of wave shoaling, breaking, and swash oscillation.

4 Discussion and Conclusions

A surf zone model has been developed for the fully nonlinear Boussinesq equations of Wei et al. (1995) and extended Boussinesq equations of Nwogu (1993) using a modified eddy viscosity model and a slot technique to represent the

moving shoreline and dry land. Comparisons with experimental data show generally good agreement, although systematic differences do exist.

The model has shown itself to predict accurately wave transformation in the surf and swash zone. Breaking phenomena are predicted both qualitatively and quantitatively for a variety of one dimensional tests. Of all tests, the greatest errors are seen for monochromatic wave shoaling and breaking on a planar beach. Here, waves heights are somewhat overpredicted before breaking. This overprediction of shoaling waves appears to be due to the the intrinsic nature of the Boussinesq equations used, which show nonlinear error in intermediate depths. Further work with higher order equations may be needed to resolve this drawback. Runup tests, on the other hand, show good agreement with experimental results for all cases considered, although some error is again visible.

5 Acknowledgements

This study has been supported by the Office of Naval Research, Base Enhancement, through the research grant N00014-97-1-0283. Many thanks are due to I.A. Svendsen and H. Mase who provided the experimental data, and H.T. Özkan-Haller who provided the runup solution, for comparisons.

6 References

Carrier, G. F. and Greenspan, H. P. (1958). "Water waves of finite amplitude on a sloping beach." *J. Fluid Mech.*, 4, 97-109.

Chen, Q., Kirby, J. T., and Dalrymple, R. A. Kennedy, B. A., Chawla, A. (1999). "Boussinesq modelling of wave transformation, breaking, and runup. II: Two horizontal dimensions." *J. Wtrwy, Port, Coast. and Oc.*

Engrg., Submitted.

Chen, Q., Kirby, J.T., Dalrymple, R.A., Kennedy, A.B., and Haller, M.C. (1998). "Boussinesq modelling of a rip current system", *J. Geophys. Res.*, Submitted.

Heitner, Heitner, K. L., and Housner, G. W. (1970). "Numerical model for tsunami runup", *J. Waterways, Ports, Coast. and Ocean Eng.*, **96**, 701-719.

Horikawa, K., and Kuo. C.-T. (1966). "A study on wave transformation inside surf zone", *Proc. Int. Conf. Coastal Eng.*, Tokyo, 217-233.

Madsen, P. A. and Schäffer, H. A. (1998). "Higher order Boussinesq-type equations for surface gravity waves - derivation and analysis", *Proc. Roy. Soc. A*, **356**, 1-59.

Madsen, P. A., and Sørensen, O. R. (1992). "A new form of the Boussinesq equations with improved linear dispersion characteristics. Part 2. A slowly varying bathymetry", *Coastal Eng.*, **18**, 183-204.

Madsen, P. A., Sørensen, O. R. and Schäffer, H. A. (1997a). "Surf zone dynamics simulated by a Boussinesq-type model. Part I. Model description and cross-shore motion of regular waves.", *Coastal Eng.*, **32**, 255-287.

Madsen, P. A., Sørensen, O. R. and Schäffer, H. A. (1997b). "Surf zone dynamics simulated by a Boussinesq-type model. Part II. Surf beat and swash oscillations for wave groups and irregular waves", *Coastal Eng.*, **32**, 289-319.

Mase, H. and Kirby, J. T. (1992). "Hybrid frequency-domain KdV equation for random wave transformation", *Proc. 23rd Int. Conf. Coastal Eng.*, Venice, 474-487.

Mase, H. (1995). "Frequency down-shift of swash oscillation compared to incident waves." *J. Hydr. Res.*, 33 (3), 397-411.

Nwogu, O. (1993). "Alternative form of Boussinesq equations for nearshore wave propagation", *J. Waterway, Port, Coast. and Ocean Engrng.*, **119**, 618-638.

Özkan-Haller H. T. and Kirby, J. T. (1997). "A Fourier-Chebyshev collocation method for the shallow water equations including shoreline runup." *Applied Ocean Res.*, 19, 21-34.

Peregrine, D. H. (1967). "Long waves on a beach", *J. Fluid Mech.*, **27**, 815-827.

Schäffer, H. A., Madsen, P. A. and Deigaard, R. A. (1993) A Boussinesq model for waves breaking in shallow water, *Coast. Engrg..*, 20, 185-202.

Svendsen, I.A., Yu, K., and Veeramony, J. (1996). "A Boussinesq breaking wave model with vorticity", *Proc.25th Int. Conf. Coastal Eng.*, Orlando, 1192- 1204.

Tao, J. (1983). "Computation of wave run-up and wave breaking", *Internal report, Danish Hydraulics Institute*, 40 pp.

Tao, J. (1984). "Numerical modelling of wave runup and breaking on the beach" *Acta Oceanologica Sinica*, 6(5), 692-700, in Chinese.

Wei, G., and Kirby, J.T., (1996). "A coastal processes model based on time-domain Boussinesq equations", *Research Report No. CACR-96-01*, Center for Applied Coastal Research, 11 pp.

Wei, G., Kirby, J. T., Grilli, S. T. and Subramanya, R. (1995). "A fully nonlinear Boussinesq model for surface waves. I. Highly nonlinear, unsteady waves", *J. Fluid Mech.*, **294**, 71-92.

Wei, G., Kirby, J. T., and Sinha, A. (1998). "Generation of waves in Boussinesq models using a source function method." *Coastal Eng.*, submitted.

Zelt, J. A. (1991). "The run-up of nonbreaking and breaking solitary waves", *Coastal Eng.*, **15**, 205-246.

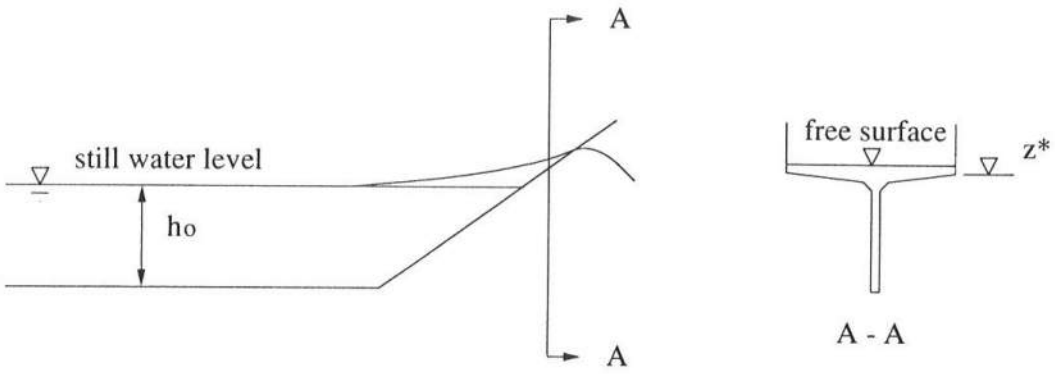

Figure 1: Schematic of a channel with the presence of a narrow slot.

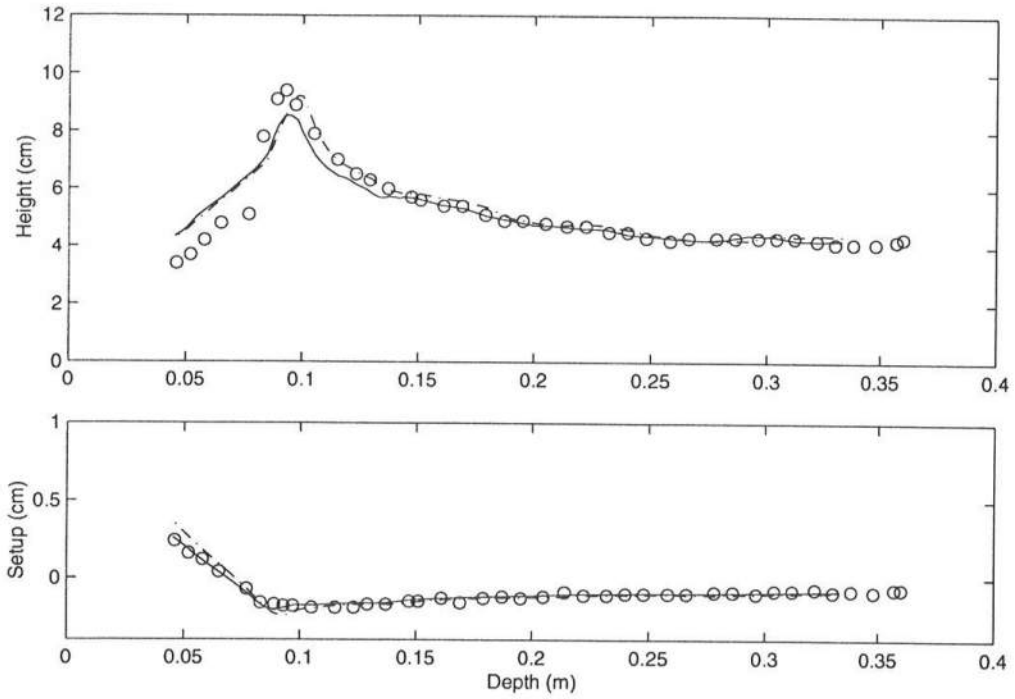

Figure 2: Computed and measured wave heights and setup for Hansen and Svendsen plunging breaker 031041; data (o); WKGS (−): Nwogu (− · −)

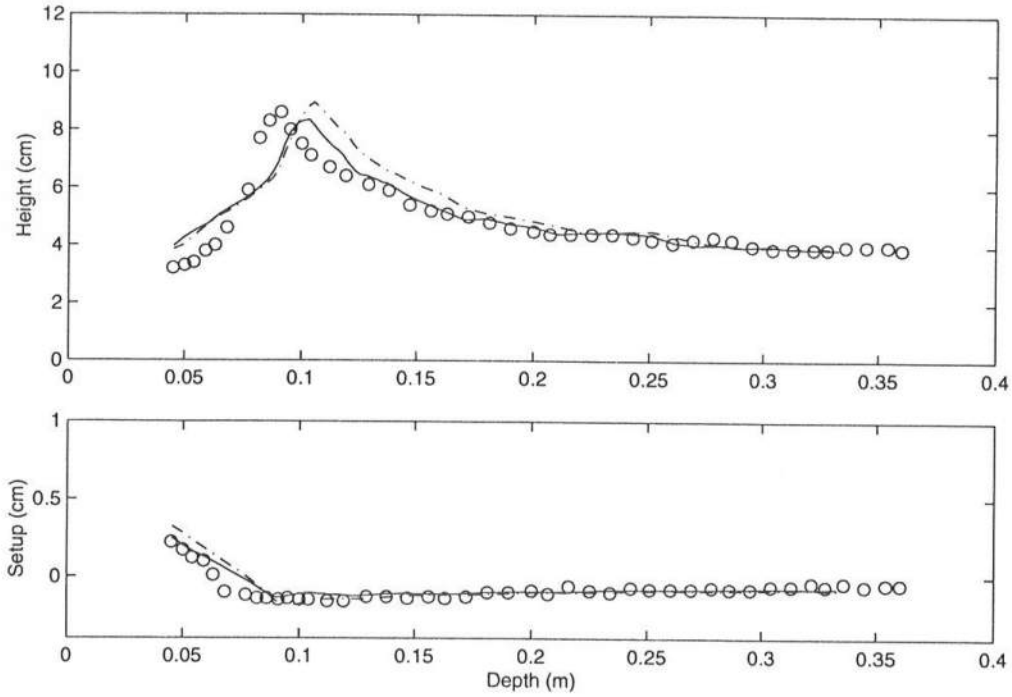

Figure 3: Computed and measured wave heights and setup for Hansen and Svendsen spilling-plunging breaker 041041; data (o); WKGS (−); Nwogu (− · −)

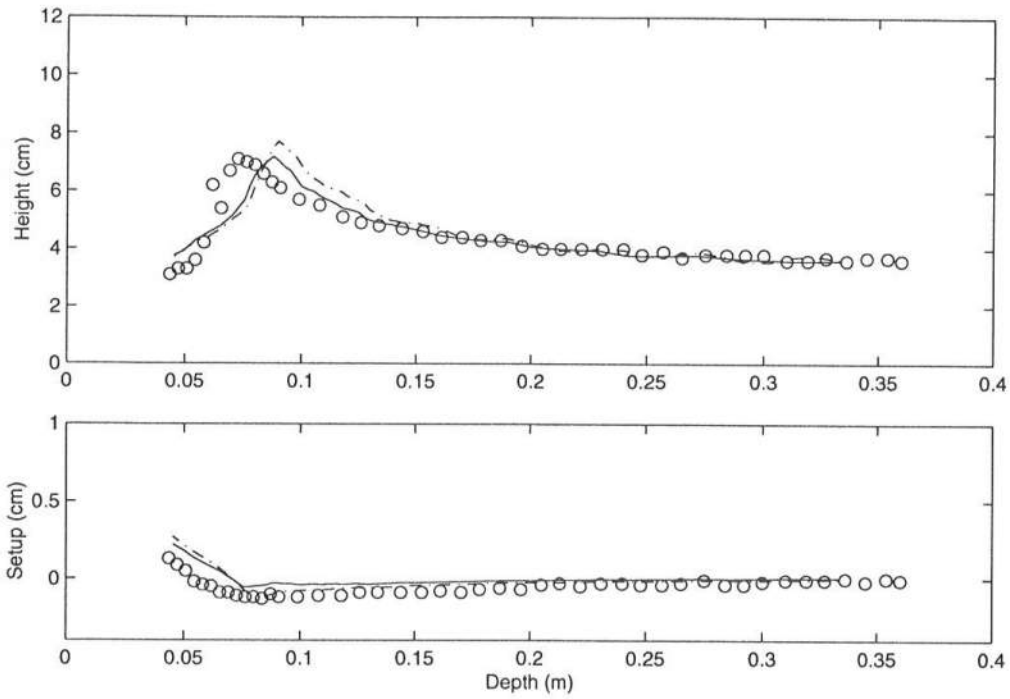

Figure 4: Computed and measured wave heights and setup for Hansen and Svendsen spilling breaker 051041; data (o); WKGS (−); Nwogu (− · −)

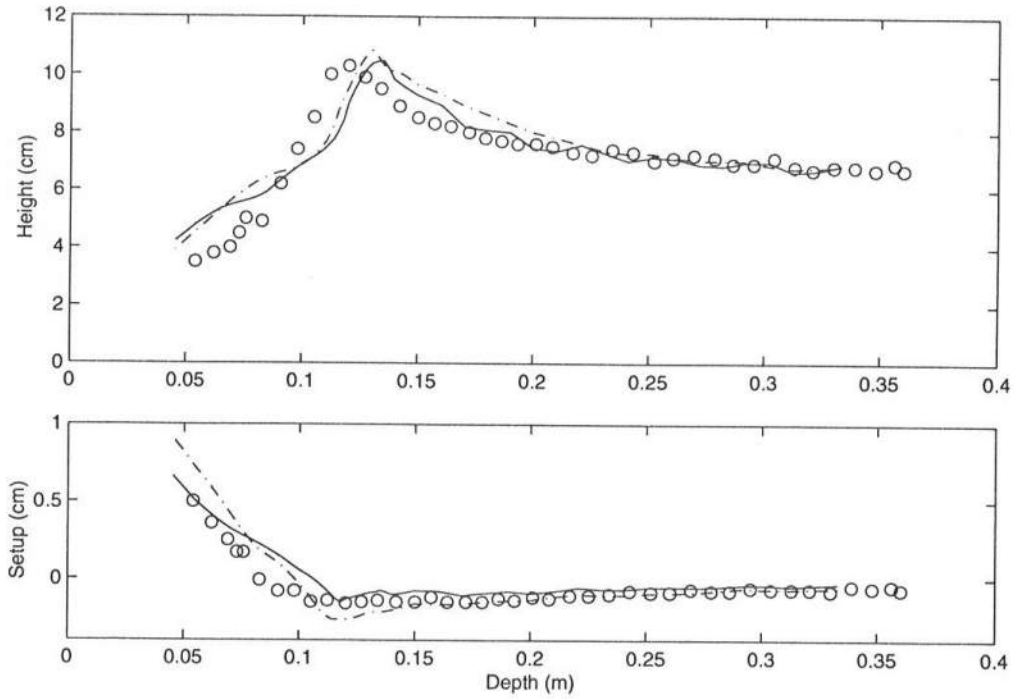

Figure 5: Computed and measured wave heights and setup for Hansen and Svendsen spilling breaker 061071; data (o); WKGS (−); Nwogu (− · −)

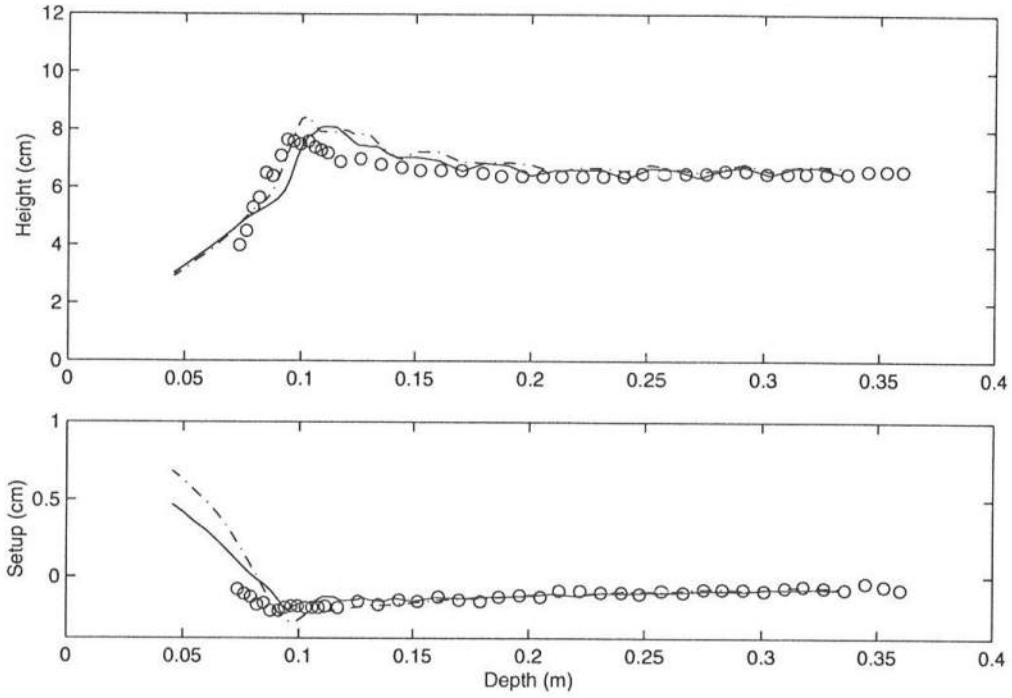

Figure 6: Computed and measured wave heights and setup for Hansen and Svendsen spilling breaker A10112; data (o); WKGS (−); Nwogu (− · −)

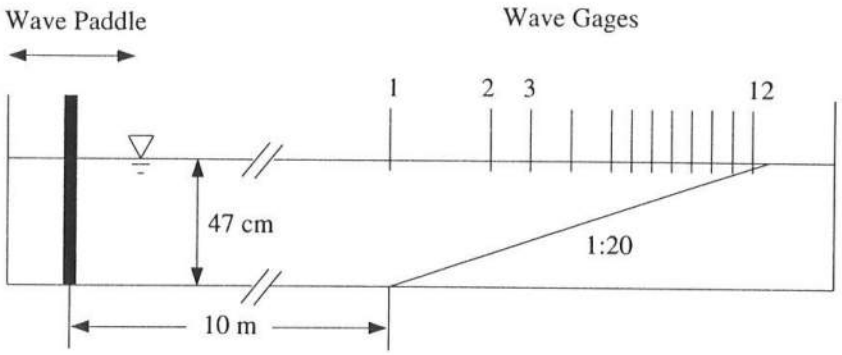

Figure 7: Schematic view of the experimental setup in Mase and Kirby (1992)

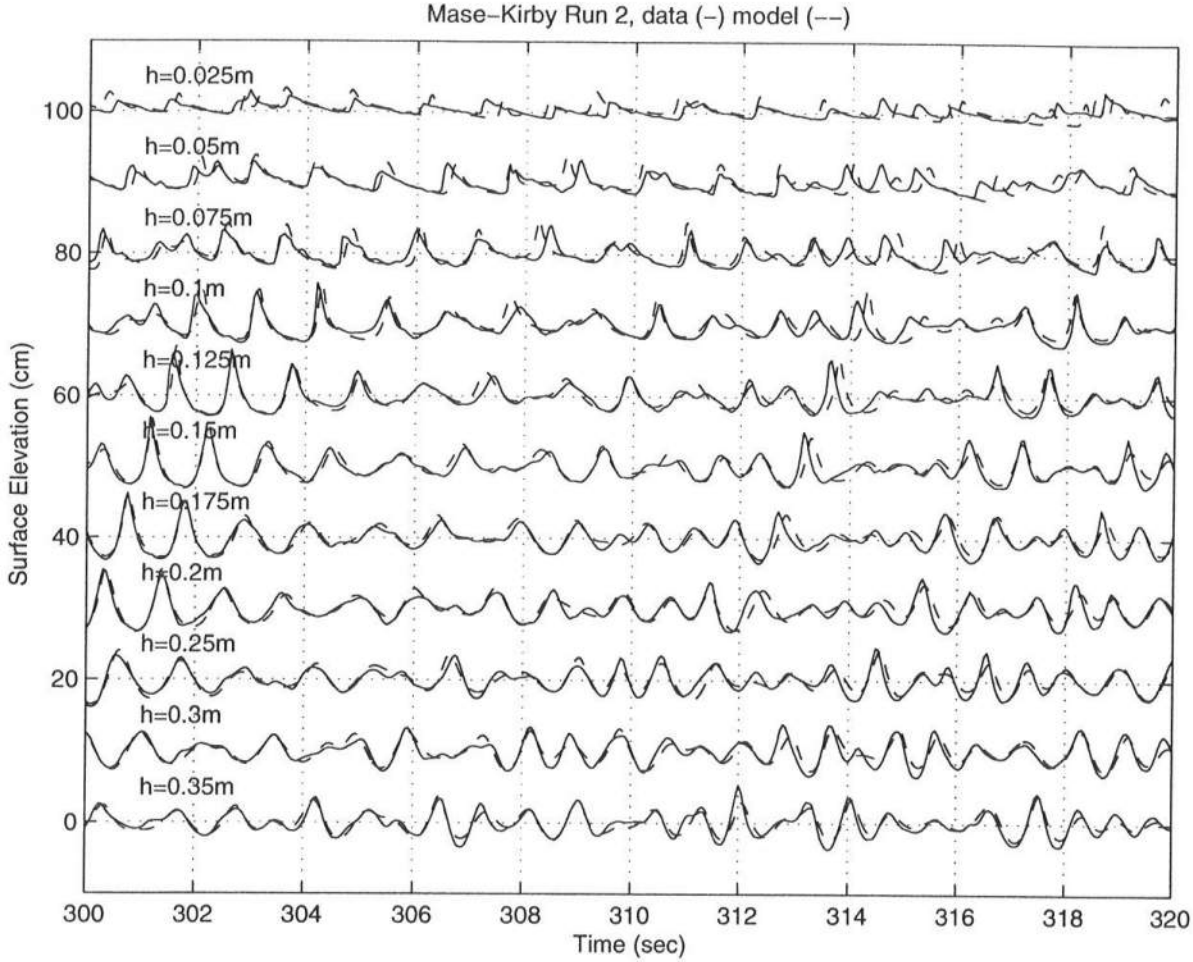

Figure 8: Time series of surface elevations for Mase and Kirby (1992) run 2, data (–), computations (– –)

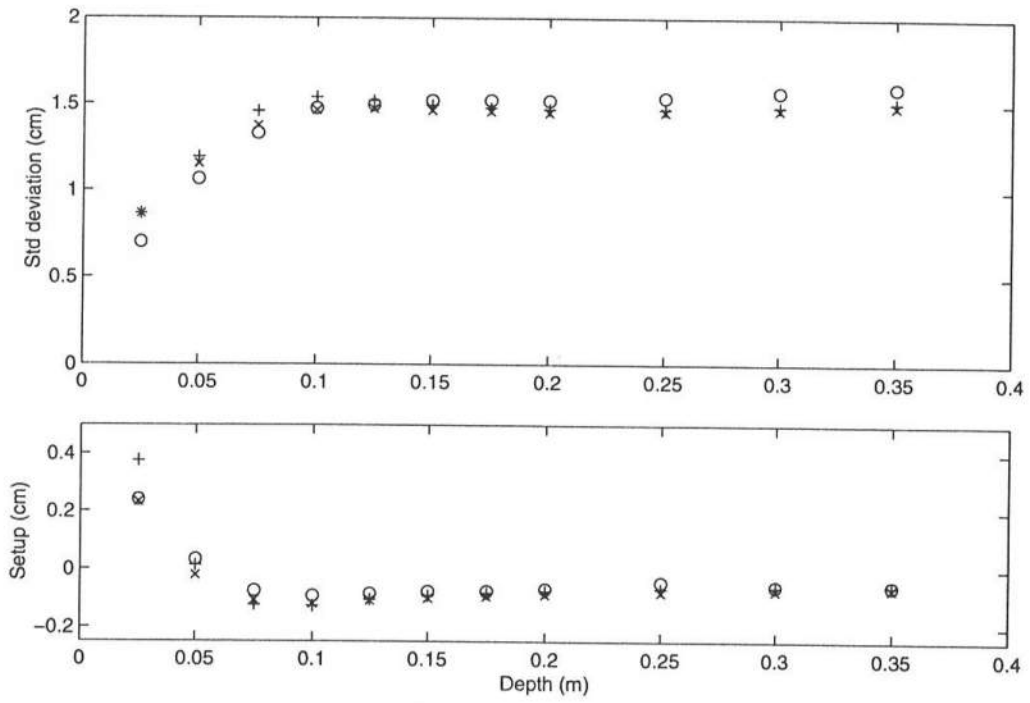

Figure 9: Computed and measured standard deviations of surface elevation, and setup for Mase and Kirby (1992) run 2; data (o); WKGS (x); Nwogu (+)

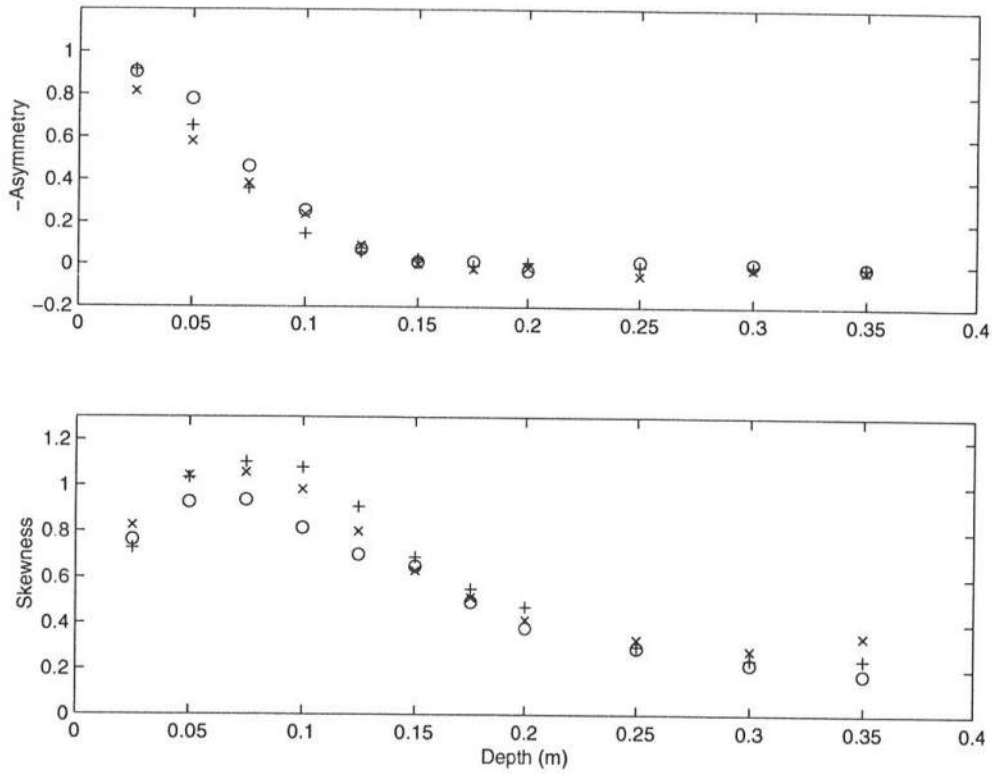

Figure 10: Computed and measured wave asymmetry and skewness for Mase and Kirby (1992) run 2; data (o); WKGS (x); Nwogu (+)

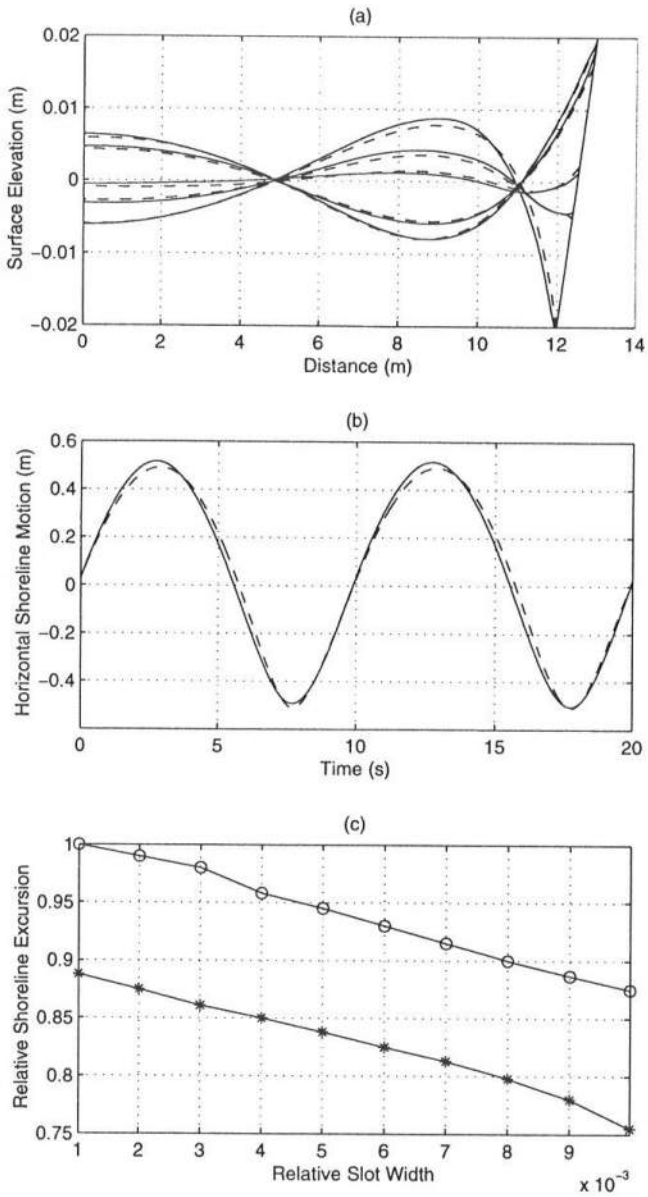

Figure 11: (a) Comparison of free surface computed by the present model (solid lines) and by Özkan-Haller and Kirby's (1997) model (dashed lines). (b) Comparison of the computed horizontal shoreline runup (solid line) and Özkan-Haller and Kirby's model result. (c) Comparison of the convergence rate of maximum shoreline excursion predicted by the improved and original slot schemes. Circles: improved; stars: original.

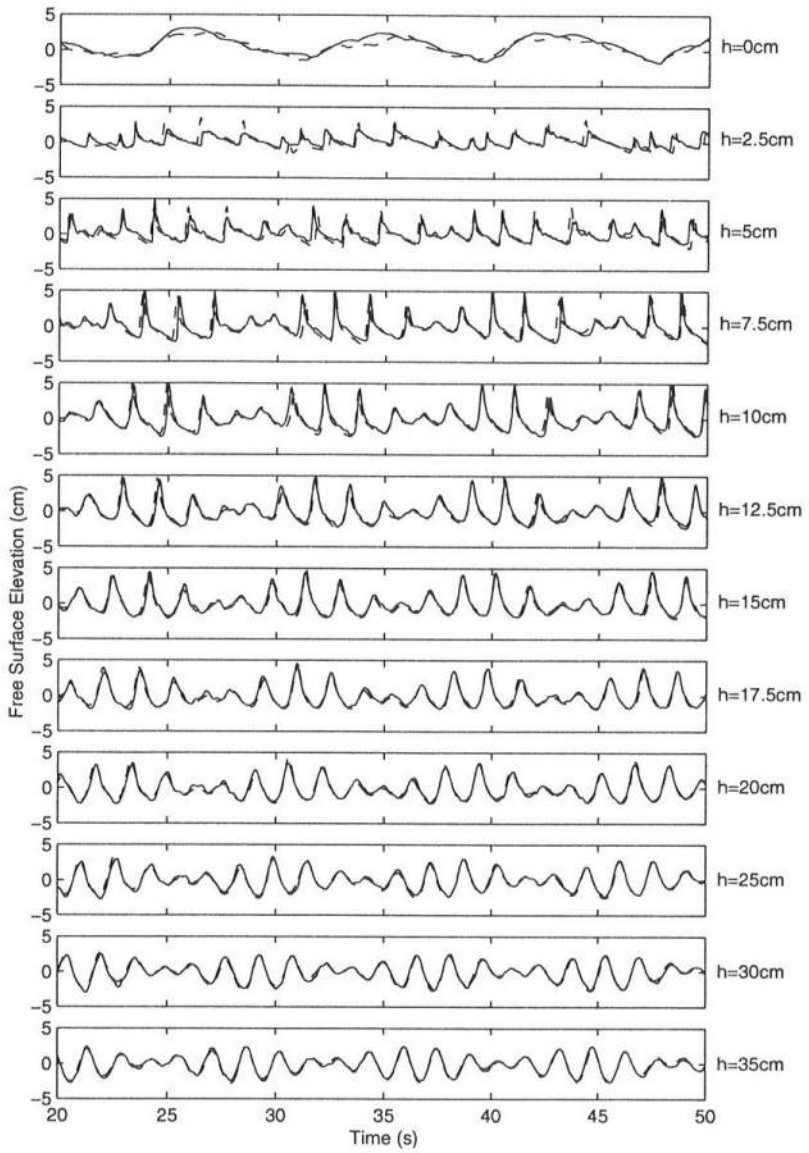

Figure 12: Comparisons of computed (dashed lines) and measured (full lines) free surface elevation including runup in Case WP1

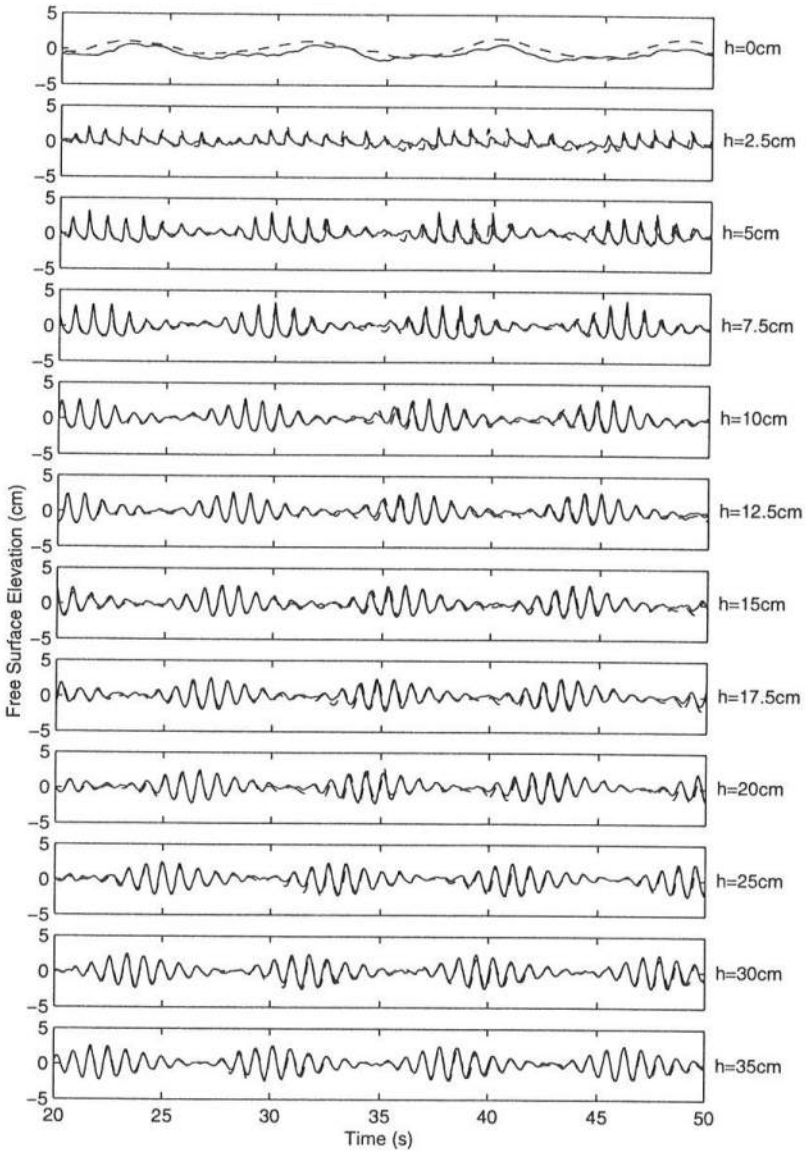

Figure 13: Comparisons of computed (dashed lines) and measured (full lines) free surface elevation including runup in Case WP2

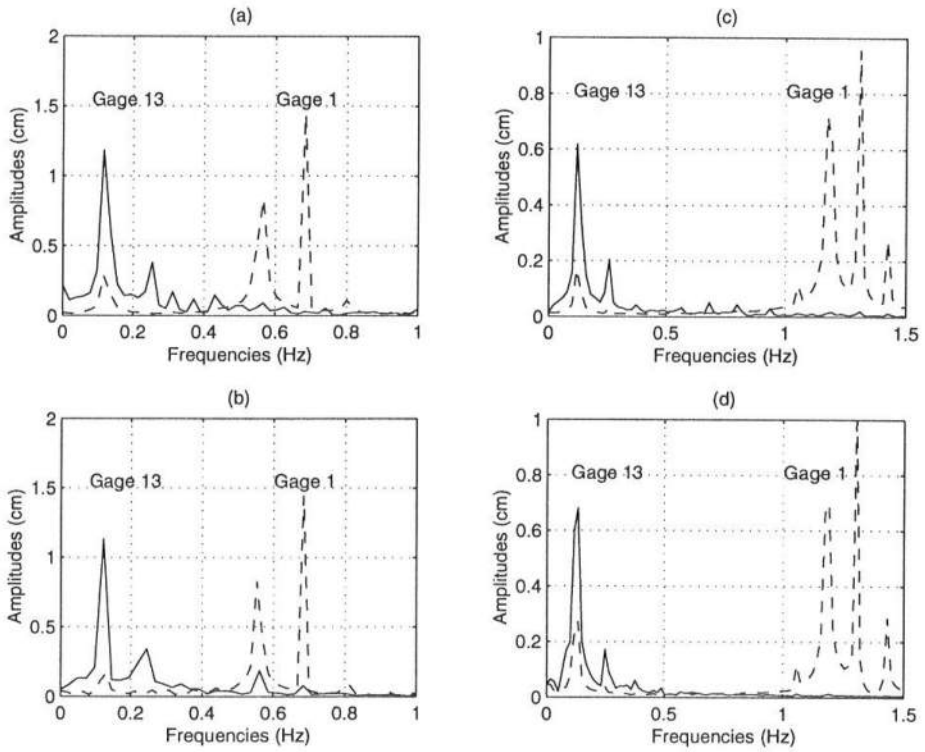

Figure 14: Comparisons of computed ((b) and (d)) and measured ((a) and (c)) frequency downshift of the swash motion. (a) and (b): Case WP1; (c) and (d): Case WP2.

BOUSSINESQ MODELING OF WAVE TRANSFORMATION, BREAKING AND RUNUP. II: TWO HORIZONTAL DIMENSIONS

By Qin Chen, [1] James T. Kirby, [2] Robert A. Dalrymple,[2]
Andrew B. Kennedy,[1] and Arun Chawla [3]

ABSTRACT

In this paper, we focus on the implementation and verification of an extended Boussinesq model for surf zone hydrodynamics in two horizontal dimensions. The time-domain numerical model is based on the fully-nonlinear Boussinesq equations (Wei *et al.*, 1995). As described in Part I (Kennedy et al., 1999), the energy dissipation due to wave breaking is modelled by introducing an eddy viscosity term into the momentum equations, with the viscosity strongly localized on the front face of the breaking waves. Wave runup on the beach is simulated using a permeable-seabed technique. We apply the model to simulate two laboratory experiments in large wave basins. They are wave transformation and breaking over a submerged circular shoal (Chawla and Kirby, 1996), and solitary wave runup on a conical island (Liu et al., 1995). Satisfactory agreement is found between the numerical results and the laboratory measurements.

[1]Postdoct. Fellow, Ctr. for Appl. Coast. Res., Dept. of Civ. and Envir. Engrg., Univ. of Delaware, Newark, DE 19716

[2]Professor, Ctr. for Appl. Coast. Res., Dept. of Civ. and Envir. Engrg., Univ. of Delaware, Newark, DE 19716

[3]Grad. Student, Ctr. for Appl. Coast. Res., Dept. of Civ. and Envir. Engrg., Univ. of Delaware, Newark, DE 19716

INTRODUCTION

An accurate model for wave-induced nearshore circulation is essential to predicting sediment and pollutant transport in coastal regions. Most of the existing numerical models for breaking-generated surf zone currents are based on vertically-integrated, time-averaged (over a short-wave period) conservation laws of mass and momentum (see Svendsen and Putrevu, 1995 for a review). The accuracy of such type of models depends on the quality of the wave transformation and breaking model that provides radiation stresses as a forcing to a circulation model. Recent advances in both computer technology and dispersive, nonlinear long wave theory (e.g. Madsen and Sørensen, 1992; Nwogu, 1993; Wei et al., 1995; Madsen and Schäffer, 1998; Chen et al., 1998) now permit the use of Boussinesq wave models for large nearshore regions and allow the averaging of model results to predict wave-induced mean flows if wave breaking is incorporated into the model. Literature reviews on advances in Boussinesq modelling of nearshore surface gravity waves can be found in Kirby (1997) and Madsen and Schäffer (1999).

The swash zone is the interface of the seawater and the land. Wave runup on the beach results in swash oscillations which are believed to cause significant sediment transport (e.g. Kamphuis, 1991). On the other hand, predicting wave runup on an open coast is important in estimating the area affected by storm waves and tsunamis. Liu et al. (1995), Titov and Synolakis (1998), among others developed numerical models for tsunami runup on the basis of nonlinear shallow water equations. Those models were tested against physical experiments carried out by Briggs et al. (1995) on solitary wave runup on a conical island. Although generally good agreement was obtained for the case of non-breaking waves, discrepancies exist in the case of broken-wave runup as shown by Liu et al., and Titov and Synolakis. This calls for models taking into account the non-hydrostatic pressure and wave breaking. Recently, Kobayashi (1998) provided a thorough literature review on wave runup on beaches

and coastal structures, and pointed out the need for research on two-dimensional shoreline runup.

The objective of this study is to implement and validate an extended time-domain Boussinesq model for wave transformation resulting from combined refaction and diffraction, wave breaking, and wave runup in two horizontal dimensions. The model is based on the fully nonlinear Boussinesq equations introduced by Wei et al. (1995).

This paper is organized as follows. Firstly, we describe the extension of the breaking and runup schemes constructed by Kennedy et al. (1999, hereafter referred to as Part I) to two horizontal dimensions. Next, the model is tested against Chawla and Kirby's (1996) physical experiment on wave propagation over a submerged circular shoal with and without breaking. Then, we use the measurements from Briggs et al.'s (1995) laboratory experiment of solitary wave runup on a conical island to validate the numerical model with respect to two dimensional shoreline runup. The results and findings are summarized in the final section.

MODEL FORMULATION

Governing Equations

The extended Boussinesq equations of Wei et al. (1995) are formulated in terms of the velocity vector $\mathbf{u}_\alpha = (u_\alpha, v_\alpha)$ at a reference elevation z_α in the water column and the free surface elevation η relative to the still water level. The equation for conservation of mass may be written as

$$\beta\eta_t + \nabla\cdot\mathbf{M} = 0 \tag{1}$$

where

$$\mathbf{M} = \Lambda\left[\mathbf{u}_\alpha + \left(\frac{{z_\alpha}^2}{2} - \frac{1}{6}(h^2 - h\eta + \eta^2)\right)\nabla\left(\nabla\cdot\mathbf{u}_\alpha\right) + \left(z_\alpha + \frac{1}{2}(h-\eta)\right)\nabla\left(\nabla\cdot\left(h\mathbf{u}_\alpha\right)\right)\right] \tag{2}$$

in which h is the still water depth, the subscript t denotes time differentiation, and ∇ is the horizontal gradient operator. In addition, β and Λ are introduced to account for the moving shoreline using the permeable-seabed technique. The detailed expressions of β and Λ can be found in Part I.

The equations for momentum conservation read

$$\mathbf{u}_{\alpha t} + \left(\mathbf{u}_\alpha\cdot\nabla\right)\mathbf{u}_\alpha + g\nabla\eta + \mathbf{V}_1 + \mathbf{V}_2 + \mathbf{R}_f - \mathbf{R}_b - \mathbf{R}_s = 0 \tag{3}$$

where g is the gravitational acceleration, and $\mathbf{V}_1$ and $\mathbf{V}_2$ are the dispersive Boussinesq terms (see Wei et al., 1995 and Part I for details). In comparison with the original momentum equations of Wei et al. (1995), there are additional terms, $\mathbf{R}_f$, $\mathbf{R}_b$, and $\mathbf{R}_s$. They are introduced for the treatment of bottom friction, wave breaking, and subgrid lateral turbulent mixing, respectively, and will be discussed in the following sub-sections. It is worth mentioning that $\mathbf{R}_b$ and $\mathbf{R}_s$ basically act as local momentum mixing due to wave breaking and unresolved turbulence. Neither of them alters the global momentum conservation. A discussion of additional model parameters may be found in Part I.

2-D Wave Breaking

Following Part I, we model the energy dissipation due to wave breaking in shallow water by introducing the momentum mixing terms $\mathbf{R}_b$ which are related to the second derivative of momentum flux. The associated eddy viscosity is essentially proportional to the gradient of the horizontal velocity and is strongly localized on the front face of the breaking wave.

Two empirical parameters are used to determine the onset and cessation of breaking. Detailed formulation of the breaking term can be found in Part I. In comparison with the 1-D breaking model, the implementation of the breaking model in two horizontal dimensions requires the determination of wave direction in order to estimate the age of a breaking event.

Assuming a primarily-progressive wave field, the application of the Sommerfeld radiation condition on a locally-constant water depth leads to an estimate of the wave direction

$$\theta = TAN^{-1}(\frac{\eta_y}{\eta_x}) \tag{4}$$

where θ is the wave incident angle relative to the x direction. Accordingly, the wave celerity vector may be written as

$$\mathbf{c} = -\frac{\eta_t}{{\eta_x}^2 + {\eta_y}^2}\nabla\eta \tag{5}$$

This is in agreement with the estimate of wave celerity in Madsen et al. (1997). With the knowledge of wave direction, the model can estimate the age of a breaking event at a given location by tracking the breaking history at the grid points along the wave ray. The remaining of the breaking model is essentially identical to the 1-D model as detailed in Part I.

There are four empirical coefficients in the breaking model. Among them are T^*, the transition time from breaking to a fully-developed bore, $\eta_t^{(I)}$ and $\eta_t^{(F)}$ which determine the onset and cessation of a breaking event. The ranges of typical values for these parameters are respectively $0.35\sqrt{gh} - 0.65\sqrt{gh}$, $0.08\sqrt{gh} - 0.15\sqrt{gh}$, and $2\sqrt{h/g} - 5\sqrt{h/g}$. The lower limit of the coefficients is found to be more suitable to bar/trough beaches while the upper limit gives optimal agreement for waves breaking on monotonic sloping beaches.

Wave Runup

Instead of tracking the moving boundary during wave runup/run-down on the beach, we treat the entire computational domain as an active fluid domain by employing an improved

version of the slot or permeable-seabed technique for simulation of wave runup. The original slot technique was proposed by Tao (1984). A variant of Tao's scheme has been used by Madsen et al. (1997) in a Boussinesq model formulated in terms of mass flux and free surface elevation.

It was shown by Madsen et al. (1997) that, even though a very narrow width of slot is used, there is still about a ten-percent error in the computed maximum runup in comparison with the analytical solution by Carrier and Greenspan (1958). This is attributed to the additional cross-sectional area introduced by the narrow slot because the maximum runup is very sensitive to the total volume of mass at the runup tip. In contrast to the original formulation that did not conserve mass in the presence of a slot, we retain an equivalent cross-sectional area of a unit width of beach, leading to the improvement in the simulation of one-dimensional runup, as shown in Part I. The extension of the runup scheme to two horizontal dimensions is straightforward. This is done by replacing the solid bottom by a narrow-slot network in the x and y directions. The resulting terms, β and Λ, in the mass equation remains identical to those in the 1-D case.

Subgrid Turbulent Mixing and Bottom Friction

In large-eddy simulation of atmospheric turbulent flow, Smagorinsky-type eddy viscosity models have been widely used to account for the contribution of unresolved small-scale motions as described in Mason (1994) and Ghosal et al. (1995). It is well known that the flow in the surf zone is characterized by eddies and turbulence generated by wave breaking. The extension of Boussinesq models based on vertically-integrated Euler equations of motion to the surf zone requires the inclusion of the turbulence effects. In addition to the energy dissipation term due to wave breaking, which is assumed to be strongly localized on the front face of the breaking wave, a parameterization of the Reynolds-like stresses resulting from

subgrid-scale turbulent processes associated with surf zone eddies may become an important factor influencing the flow pattern of the wave-generated current field. In the absence of a subgrid model in the governing equations, the underlying current field generated by wave breaking may become so chaotic that no realistic flow pattern can be recognized as observed in our numerical experiments of rip current generation on a barred beach. we therefore utilize a Smagorinsky-type subgrid model (Smagorinsky et al. 1965) to account for the effect of the resultant eddy viscosity on the underlying flow. The detailed formulation is given in Chen et al. (1999).

The bottom friction is modelled by the use of the quadratic law

$$\mathbf{R_f} = \frac{f}{h+\eta}\mathbf{u}_\alpha|\mathbf{u}_\alpha| \tag{6}$$

where f is the bottom friction coefficient. In the literature, the value of f varies significantly. For instance, the coefficient used by Zelt (1991) in his Boussinesq model for solitary wave runup on a 1:20 sloping bottom is two orders of magnitude smaller than the coefficients used to compute longshore currents generated in laboratories (e.g. $f \approx 1.0 \times 10^{-2}$) in Kobayashi et al. (1997). Numerical experiments indicate that the present model is not very sensitive to the choice of friction coefficient in the simulation of rip current generation on a barred beach with rip channels (Chen et al., 1999). Care should be taken, however, when chose bed shear stress coefficients for modelling wave-induced alongshore currents. Under field conditions, owing to the variability of hydrodynamic and morphologic characteristics, spatially-variable friction coefficients (e.g. $f \approx 1.0 \times 10^{-3}$ *to* 5.0×10^{-3}) are likely to be used, as shown by Whitfor and Thornton (1996) who inferred the bed shear stress coefficients for longshore currents over a barred profile on the basis of momentum balance in alongshore direction.

Following Wei et al. (1995), quasi fourth-order finite difference schemes are used to solve the governing equations described above. An analysis of the linear stability and other properties of the numerical scheme can be found in Wei (1997).

WAVE TRANSFORMATION OVER A CIRCULAR SHOAL

Model Set-up

A series of physical experiments for wave transformation over a circular shoal was conducted by Chawla and Kirby (1996) in the directional wave basin at the University of Delaware. Their measurements provide good test cases for model/data comparison. Figure 1 shows the plan view of the wave basin with the transects of wave gauge locations. The physical wave basin is approximately 18 m long and 18.2 m wide. A circular shoal was placed on an otherwise flat bottom in the basin. For detailed description of the experiment, the reader is referred to Chawla and Kirby (1996).

Accordingly, the numerical wave basin is chosen to be 20 m long and 18.2 m wide. On the western boundary, monochromatic waves are generated by the source function technique developed by Wei et al. (1999). Near the eastern wall of the wave basin, a 3 m wide sponge layer is used, which represents a sloping stone beach in the physical experiment. The center of the shoal is located at $x = 5\ m$ and $y = 8.98\ m$. The perimeter of the shoal is given by

$$(x-5)^2 + (y-8.98)^2 = (2.57)^2 \tag{7}$$

and the water depth on the submerged shoal is given by

$$h = h_o + 8.73 - \sqrt{82.81} - (x-5)^2 - (y-8.98)^2 \tag{8}$$

in which h_o is the water depth of the wave basin.

Chawla and Kirby's (1996) laboratory experiments consist of test cases of regular waves and directional random waves, including breaking and non-breaking cases. To verify the basic properties of the Boussinesq model with respect to combined refraction/diffraction and

wave breaking in two horizontal dimensions, only the data sets of monochromatic waves are used in the present study. Emphasis will be given to the test case with wave breaking.

Model/Data Comparison: Non-breaking Waves

In the case of non-breaking wave transformation over submerged shoals, the Boussinesq model based on the fully-nonlinear equations introduced by Wei et al. (1995) was verified against the laboratory experiments of Berkhoff et al. (1982) and Chawla and Kirby (1996). Excellent agreement between the model results and measurements has been found (see Wei, 1997). For illustration, we present the comparison of the model results with one of the Chawla and Kirby's (1996) tests (Test 4).

The wave height at the input boundary is 1.18 cm and the wave period is 1.0 s. The flat bottom of the basin has a water depth $h_o = 45$ cm leading to $h = 8$ cm on the top of the circular shoal. We choose the grid spacing to be 0.05 m and 0.1 m in the x (incident wave direction) and y directions, respectively. The time step is 0.01 second. The model is run for 40 seconds and the wave field reaches a steady condition. We compute the root-mean-square wave heights (H_{rms}) based on the time series of the last 10 seconds of data although the waves are mainly periodic. Figure 2 shows the comparison of the modelled and measured H_{rms} along seven transects covering most the areas of the submerged shoal and behind the shoal (see Fig. 1). Excellent agreement is observed.

In Fig. 2, solid lines represent the Boussinesq model results while circles are the measurements, which are normalized by the incident H_{rms}. Along the longitudinal transect A-A (y = 8.98 m), the Boussinesq model predicts very well the wave shoaling and focusing and the decrease of wave height after the shoal. In comparison with Berkhoff et al.'s (1982) elliptic shoal which is placed on a sloping beach, the topography in Chawla and Kirby's (1996) ex-

periments leads to much stronger wave focusing. For instance, the maximum amplification factor of wave height reaches about 2.7 on top of the shoal in the present simulation. We notice that the Boussinesq model also correctly simulates the transverse variation of the wave field resulting from the effects of combined refraction/diffraction as shown by the good agreement along the transects from B-B to G-G. Owing to a slight off-centering of the shoal position (slightly closer to one of the side walls), the distribution of the wave height in the y direction is not symmetric. This signature of asymmetry is also accurately predicted by the Boussinesq model.

Model/Data Comparison: Breaking Waves

A more demanding test for the Boussinesq model is wave propagation and breaking over a submerged shoal. We choose another test case from Chawla and Kirby's (1996) experiment with wave breaking to verify our model. In this case, the water depth h_o is 39.5 cm. The input monochromatic wave has 2 cm wave height and 1 s period. As the front face of a breaking/broken wave becomes very steep, finer grid size in comparison with that for the case of non-breaking is required in order to resolve the wave. Thus we reduce the grid size in the x direction to 0.025 m, leading to about 20 grids per wave length on top of the submerged shoal, while the grid increment along the y axis and the time step remain identical to those in the case of non-breaking waves.

The Boussinesq model is run for 50 seconds of simulated time. To remove the effects of transients associated with the cold start of wave field and the wave breaking, we compute the H_{rms} using the last 20 seconds of numerical results and the collected data. The empirical parameters for the wave breaking model are chosen to be the lower limit of the values indicated in the preceding section. Figure 3 presents the comparisons of the modelled results and measurements along the longitudinal transect (A-A) with respect to the normalized H_{rms},

skewness and asymmetry. The computed H_{rms} and third-moments agree fairly well with the laboratory data.

The bottom topography along the A-A transect is shown by Fig. 3d. Several interesting phenomena are observed from Fig. 3. First, we notice that the wave height does not reach the largest on top of the shoal but on the downward slope instead. This is attributed to the focusing effect of wave refraction on the shoal. However, the wave skewness and asymmetry appear to be the maximum near the crest of the shoal, as indicated by both the numerical and measured results. It is known that skewness and asymmetry are a measure of wave nonlinearity. Apparently, the degree of wave nonlinearity at the focusing point with the maximum wave height is weaker than that on top of the shoal where the water depth is the minimum. Secondly, both depth-limited wave breaking and wave de-focusing reduce the wave height. The combined decrease of wave height is much faster in comparison with the case of non-breaking waves. Consequently, the large gradient of radiation stresses will drive horizontal circulations around the submerged shoal.

Figure 4 depicts the data/model comparison of normalized H_{rms} along six transverse transects. On top of the shoal (i.e. F-F), agreement is fairly good. On the downward slope, the Boussinesq model captures the focusing effects very well as shown by E-E transect. Furthermore, the de-focusing and diffraction of the broken waves behind the shoal (i.e. B-B to D-D) are also predicted reasonably well by the Boussinesq model.

A computed wave field at the end of the simulation is shown in Fig. 5a where the gray areas represent the modelled wave crests while the dark areas are the wave troughs. Wave crests become very peaky (narrower and brighter in the figure) on the top of the shoal due to nonlinear shoaling effects. Secondly, wave refaction over the shoal is clearly shown by the bending of wave crests on top of the shoal. Wave diffraction is also visible by the variation

of wave crests in the transverse direction. It is worth mentioning that secondary wave crests are observed behind the submerged shoal due to the release of superharmonics generated by nonlinear shoaling. However, their phases may be inaccurate because of the large wave numbers of the higher harmonics at those locations. Model equations with Pade [4,4] dispersion properties applicable to $kh = 6$ (e.g. Chen et al., 1998, Madsen and Schäffer, 1998, Gobbi et al., 1999) would permit a better estimate of the released, free, higher harmonics in these two test cases.

There is no measurement of breaking-induced circulation in Chawla and Kirby's (1996) experiments. However, a strong jet associated with wave breaking on top of the shoal was visually observed during the experiment. Information on wave-induced circulation in the simulation can be extracted using a short averaging window to filter out the orbital wave motion. Figure 5b illustrates the underlying current field generated by wave breaking over the shoal after 50 seconds have elapsed in the simulation. The current field is obtained by averaging the instantaneous fluid particle velocity at the reference level z_α over two wave periods. In connection with the simulation of breaking-induced currents, the bottom friction coefficient of $f = 1.0 \times 10^{-4}$ and a subgrid mixing model is used. Notice that the jet-like current tends to be unstable and vortices are likely to appear as shown by the meandering of the computed current and the vortex pair. An account of the instability of jet-like rip currents and the mechanism of vortex generation is given in Chen et al. (1999).

WAVE RUNUP ON A CONICAL ISLAND

Briggs et al.'s (1995) laboratory experiment on solitary wave runup on a conical island has served as a benchmark for the verification of tsunami runup models (see e.g. Liu et al., 1995; Titov and Synolakis, 1998). We shall use the measurements from their physical experiment to validate our runup schemes for two horizontal dimensions. In the case of one

dimensional runup, the present model was tested against an analytical solution by Carrier and Greenspan (1958) and a wide range of experimental data including irregular waves. Good agreement has been obtained as shown in Part I.

A schematic view of the wave basin for Briggs et al.'s (1995) experiments is shown in Fig. 6 where solitary waves are generated on the western boundary and propagate toward the eastern boundary. The wave basin is 25 m long and 30 m wide. A conical island with a slope of 1:4 is placed on an otherwise flat bottom in the basin. The center of the island is located at $x = 13$ m and $y = 15$ m. The diameters of the island on the bottom, at the still water line, and on the top are respectively 7.2 m, 4.64 m, and 2.2 m. The water depth of the basin is 0.32 m. Further information about the experiment set-up can be found in Briggs et al. (1995) and Liu et al. (1995).

There are three test cases with available data sets including measurements of maximum runup height and free surface elevation around the island. The initial conditions for the three cases have $\epsilon = 0.05$, 0.1 and 0.2, respectively, where ϵ denotes the height-to-depth ratio of the incident solitary waves. The water depth remain the same in all three cases. We set up our numerical model by choosing the grid size to be 0.1 m in both x and y directions. A 0.02 second is used as the time step. We generate solitary waves by defining the initial conditions for the model based on the analytical solutions to the Boussinesq equations with a constant water depth (see Wei, 1997). The crest of the solitary waves at $t = 0$ is located at $x = 0.0$. At the four lateral boundaries, closed boundaries are imposed.

Figure 7 presents model/data comparisons of the maximum runup heights around the island for the three test cases. The full lines represent the numerical results while stars denote the data measured by Briggs et al. (1995). The horizontal axis is the angles between the radius and the center line of the island in the incident wave direction, 0 degrees correspond-

ing to the front side of the island while 180 degrees corresponding to the lee side. Runup heights are normalized by the height of the incident solitary wave. As the measurements show that the maximum runup heights are not perfectly symmetric about the center line of the island, we compare the numerical results with the average of the data on both sides of the center line aligned with the incident wave direction. Good agreement between the model predictions and the measurements is observed. The runup scheme captures the signature of two dimensional runup as shown by the correct variation of the runup heights around the island. As mentioned in the introductory section, Case 3 is a challenging test because of inaccurate prediction by non-dispersive models without the consideration of wave breaking. Although a slight discrepancy is found on front side of the island in the comparison of Case 3, the overall agreement is as good as for the non-breaking cases.

In addition to the distribution of maximum runup heights, we compare the computed time series of free surface with the measurements at five locations. Gauge 3 is located close to the input boundary while the other four gauges are around the island near the still water shoreline. Figures 8, 9 and 10 show the comparisons corresponding to Cases 1, 2 and 3, respectively.

First, we notice that the computed primary waves agree reasonably well with the measurements for all three cases. The Boussinesq equations give a better description of the solitary wave than the non-dispersive shallow water equations do. This becomes more clear in Case 3 when we compare our model with Titov and Synolakis' (1998) numerical results that had remarkable discrepancies compared with the measured time series of free surface. For instance, secondary crests on the back side of the leading waves as predicted by the non-dispersive model are absent in gauges 3-16 of both the measurements and Boussinesq model results. Secondly, the present model predicts reasonably well the free surface on the lee side of the island as shown by Gauge 22. In contrast, the non-dispersive model tends

to under-estimate the leading wave height behind the island as demonstrated by Titov and Synolakis (1998).

The present model with permeable-seabed technique for shoreline runup, however, appears to under-predict the depression of the free surface, or the reflected waves by the island. This is shown by the model/data comparison of Gauge 9 located in front of the island. The discrepancy is attributed to the slight loss of wave energy and momentum because of the presence of the narrow slot. Owing to the very steep slope of the island (1:4) and the high nonlinearity of the solitary waves in Cases 2 and 3, a slot width ten times larger than the optimal values as found in Part I. are used here for the concerns of numerical instability. A low pass filter localized in the swash region is also utilized to suppress possible noise due to the use of a slot. It is worth mentioning that phase differences between the computed and measured free surface at Gauge 1 in Cases 1 and 3 are due to a slight variation of the gauge location in the physical experiment as described in Briggs et al. (1995).

As discussed in Liu et al. (1995), a collision of the trapped solitary waves on the lee side of the island could lead to a runup height which can exceed the maximum runup on the front side of the island. Figure 11 illustrates the collision process in Case 2. The time sequence of the computed free surface shows the scenario of head on collision of the trapped solitary waves on the lee side of the island. Figure 12 depicts the maximum runup on the lee side of the island in Case 3 with a larger incident solitary wave in comparison with the other two cases. It is noticed that the computed maximum water surface elevation which is considered as the maximum runup height in Case 3 is separated from the island slope. This separation does not occur in Cases 1 and 2. As observed in the physical experiment, the collision of the trapped waves on back side of the island in Case 3 caused wave breaking and very rough water surface. The breaking model is not expected to be able to simulate the mixing of a backward propagation bore on the lee side of the island. Nevertheless, the generally good

agreement of comparisons in this section demonstrates the capability of the model for the simulation of shoreline runup in two horizontal dimensions.

SUMMARY AND CONCLUSIONS

A numerical model based on the fully-nonlinear Boussinesq equations (Wei et al., 1995) has been extended to include wave breaking and moving shorelines for the simulation of nearshore wave transformation with wave breaking, two-dimensional swash motion, and wave-induced horizontal circulation. Fully-coupled wave/current interaction is taken into account by the Boussinesq equations. The model not only predicts the nearshore propagation of nonlinear surface gravity waves, but also gives the underlying unsteady flow generated by wave breaking. The current field is obtained directly by time averaging the computed instantaneous fluid particle velocity over a certain period of time.

The model results are compared with the measurements from two large scale laboratory experiments on wave transformation over a submerged circular shoal with and without wave breaking (Chawla and Kirby, 1996), and solitary wave runup on a conical island (Briggs et al., 1995). Generally good agreement is observed between the laboratory data and the numerical results, including spatial variation of root-mean-square wave heights and distribution of maximum runup heights.

The numerical model predicts well the combined refraction and diffraction of nonlinear waves with wave breaking over rapidly varying bathymetry. Model/data comparisons also show that, for shoaling and runup of solitary waves, the Boussinesq model gives better predictions than do non-dispersive models based on nonlinear shallow water equations in the literature. The two dimensional version of the breaking and runup schemes work reasonably well. This model has been successfully used by Chen et al. (1999) to simulate a rip current

system on a barred beach with rip channels in the laboratory. Good agreement has been found between numerical predictions and measurements, including wave height, mean water level, and alongshore and cross-shore currents.

ACKNOWLEDGEMENTS

This study has been supported by the Office of Naval Research, Base Enhancement Program, through the research grant N00014-97-1-0283. J.T. Kirby and A. Chawla's work was also supported by the NOAA Office of Sea Grant, Department of Commerce, under Grant No. NA/6RG0162-01. Many thanks are due to Michael J. Briggs who provided the experimental data for comparisons.

REFRENCES

Berkhoff, J. C. W., Booy, N. and Radder, A. C. (1982). "Verification of numerical wave propagation models for simple harmonic linear water waves.", *Coast. Engrg.*, 6, 255-279.

Briggs, M. J., Synolakis, C.E., and Harkins, G. S.(1994). "Tsunami run-up on a conical island." *Proc. Waves - Physical and Numerical Modelling*, Vancouver, Canada, 446-455.

Carrier, G. F. and Greenspan, H. P. (1958). "Water waves of finite amplitude on a sloping beach." *J. Fluid Mech.*, 4, 97-109.

Chawla, A. and Kirby, J. T. (1996). "Wave transformation over a submerged shoal." *CACR Rep. No. 96-03*, Dept. of Civil Engrg., University of Delaware, Newark, DE.

Chen, Q., Madsen, P. A., Schäffer, H. A., and Basco, D. R. (1998). "Wave-current interaction based on an enhanced Boussinesq approach." *Coast. Eng.*, 33, 11-39.

Chen Q., Dalrymple, R. A., Kirby, K. T., Kennedy, A. B., and Haller, M. C. (1999). "Boussinesq modelling of a rip current system." *J. Geophys. Res.*, Submitted.

Ghosal, S., Lund, T. S., Moin, P., and Akselvoll, K. (1995). "A dynamic localization model for large-eddy simulation of turbulent flows." *J. Fluid Mech.*, 186, 229-255.

Gobbi, M. F., Kirby, J. T., and Wei, G. (1999). "A fully nonlinear Boussinesq model for surface waves. II. Extension to $O(kh^4)$." *J. Fluid Mech.*, submitted.

Kamphuis, J. W. (1991). "Alongshore sediment transport rate." *J. Wtrwy., Port, Coast. and Oc. Engrg.,* ASCE, 117(6), 624-640.

Kennedy, A. B., Chen, Q., Kirby, J. T., and Dalrymple, R. A. (1999). "Boussinesq modelling of wave transformation, breaking, and runup. I: One dimensional motions." *J. Wtrwy, Port, Coast. and Oc. Engrg.*, Submitted.

Kirby, J. T. (1997). "Nonlinear, dispersive long waves in water of variable depth." in *Gravity Waves in Water of Finite Depth*, edited by J.N. Hunt, Computational Mechanics Publications, 55-126.

Kobayashi, N., Karjadi, E. A., and Johnson, B. D. (1997). "Dispersion effects on longshore currents in surf zones." *J. Wtrwy, Port, Coast. and Oc. Engrg.*, 123(5), 240-248.

Kobayashi, N. (1999). "Wave runup and overtopping on beaches and coastal structures." in *Advances in Coast. and Ocean Engrg.*, Edited by P.L.-F. Liu, in press.

Liu, P. L.-F., Cho, Y.-S., Briggs, M. J., Kanoglu, U., and Synolakis, C. E. (1995). "Runup of solitary waves on a circular island." *J. Fluid Mech.*, 302, 259-285.

Madsen, P. A., and Sørensen, O. S. (1992). "A new form of the Boussinesq equations with improved linear dispersion characteristics. Part 2. A slowly varying bathymetry." *Coast. Engrg.*, 18, 183-204.

Madsen, P. A., Sørensen, O. R., and Schäffer, H. A. (1997). "Surf zone dynamics simulated by a Boussinesq-type model. Part I. Model description and cross-shore motion of regular waves." *Coast. Engrg.*, 32, 255-287.

Madsen, P. A., and Schäffer, H. A. (1998). "Higher order Boussinesq Boussinesq-type equations for surface gravity waves: Derivation and analysis." *Philos. Trans. R. Soc. London*, Ser. A., Vol. 356, 1-59.

Madsen, P. A., and Schäffer, H. A. (1999). "A review of Boussinesq-type equations for gravity waves." in *Advances in Coast. and Ocean Engrg.*, Edited by P.L.-F. Liu, World Scientific. in press.

Mason, P. (1994). " Large-eddy simulation: a critical review of the technique." *Q. J. R. Meteorol. Soc.*, 120, 1-26.

Nwogu, O. (1993). "Alternative form of Boussinesq equations for nearshore wave propagation." *J. Wtrwy, Port, Coast. and Oc. Engrg.*, 119, 618-638.

Smagorinsky, J., Manabe, S., Holloway, J. L. (1965). "Numerical results from a nine-level general circulation model of the atmosphere." *Mon. Weather Rev.*, 93, 727-768.

Svendsen, I. A., and Putrevu, U. (1995). "Surf-zone hydrodynamics." in *Advances in Coast. and Ocean Engrg.*, Edited by P. L.-F. Liu, 2, 1-78.

Tao, J. (1984). "Numerical modelling of wave runup and breaking on the beach." *Acta Oceanologica Sinica*, 6(5), 692-700, in Chinese.

Titov, V. V., Synolakis, C. E. (1998). "Numerical modeling of tidal wave runup." *J. Wtrwy, Port, Coast. and Oc. Engrg.*, 124 (4), 157-171.

Wei, G., Kirby, J. T., Grilli, S. T., and Subramanya, R. (1995). "A fully nonlinear Boussinesq model for surface waves. Part 1: Highly nonlinear unsteady waves." *J. Fluid Mech.*, 294,71-92.

Wei, G. (1997). "Simulation of water waves by Boussinesq models." *Ph.D. Thesis*, Dept. of Civil Engrg., Univ. of Delaware, Newark, DE.

Wei, G., Kirby, J. T., and Sinha, A. (1999). "Generation of waves in Boussinesq models using a source function method." *Coast. Engrg.*, submitted.

Zelt, J. A. (1991). "The run-up of nonbreaking and breaking solitary waves." *Coast. Engrg*, 15, 205-246.

Whitford, D. J., and Thornton, E. B. (1996). "Bed shear stress coefficients for longshore currents over a barred profile". *Coast. Engrg*, 27, 243-262.

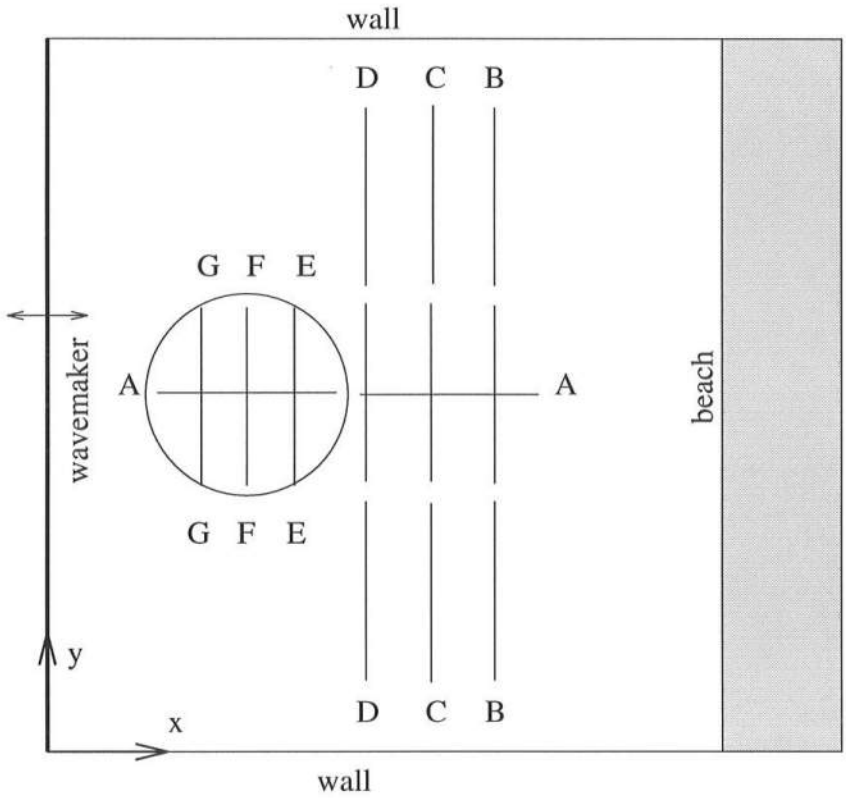

Figure 1: Schematic View of Chawla and Kirby's (1996) Experimental Setup and Transects of Wave Gauge Locations

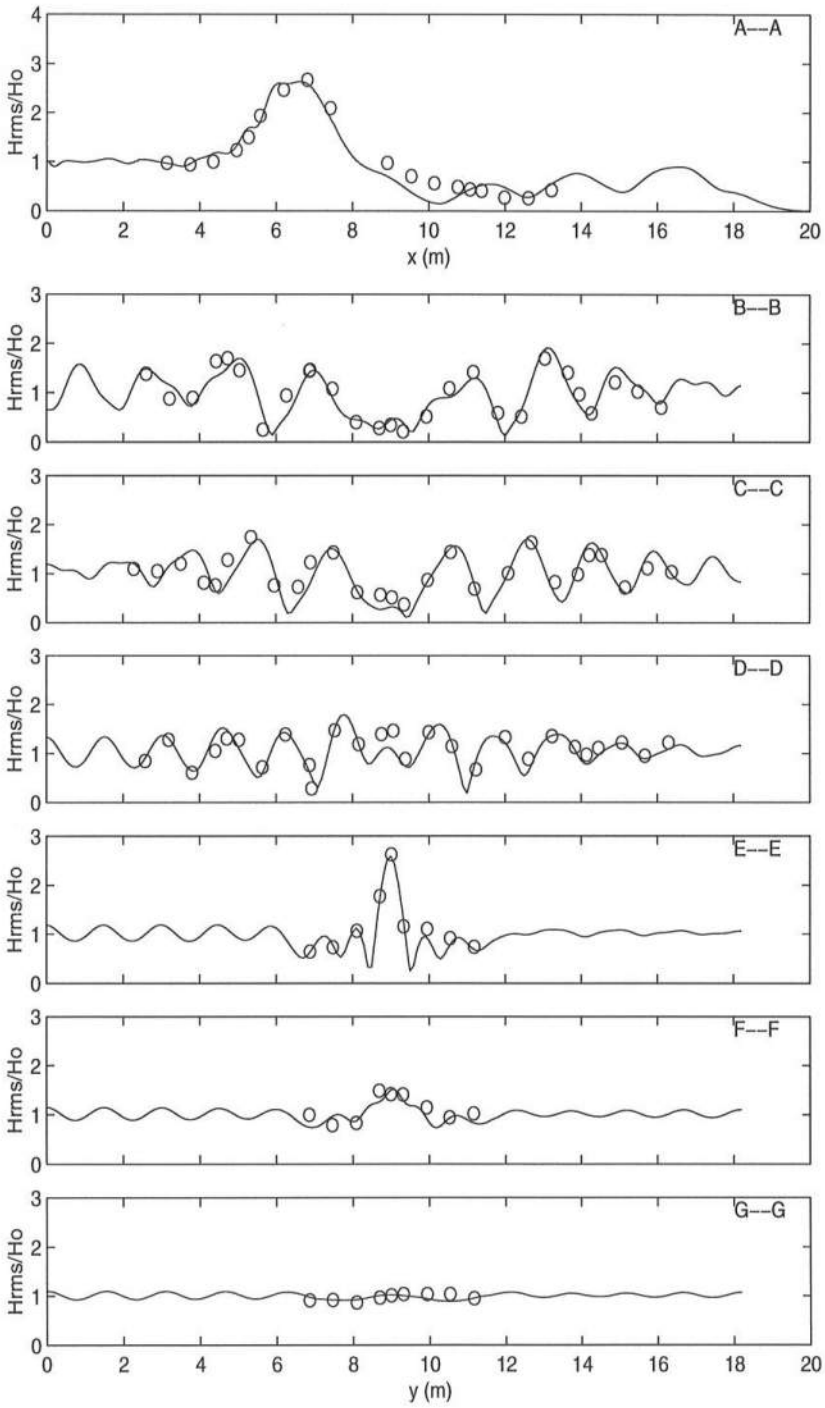

Figure 2: Comparisons of Computed H_{rms} and Chawla and Kirby's (1996) Measurements. Solid Lines: Model; Circles: Data. Non-breaking waves, Test 4.

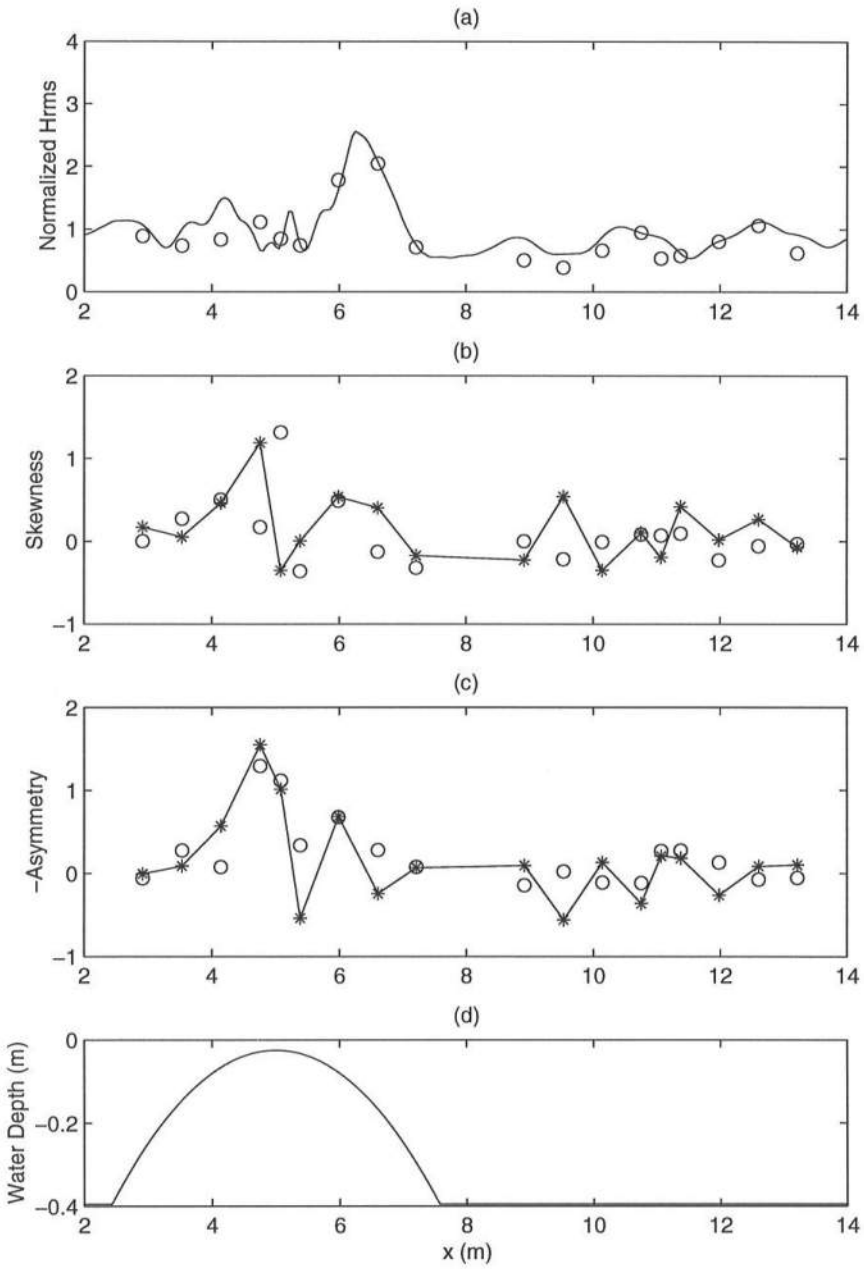

Figure 3: Model/Data Comparisons along A-A Transect: (a) Normalized H_{rms}; (b) Normalized Skewness; (c) Normalized Asymmetry; (d) Bottom Topography. Solid Lines: Model; Circles: Data. Breaking waves, Test 4.

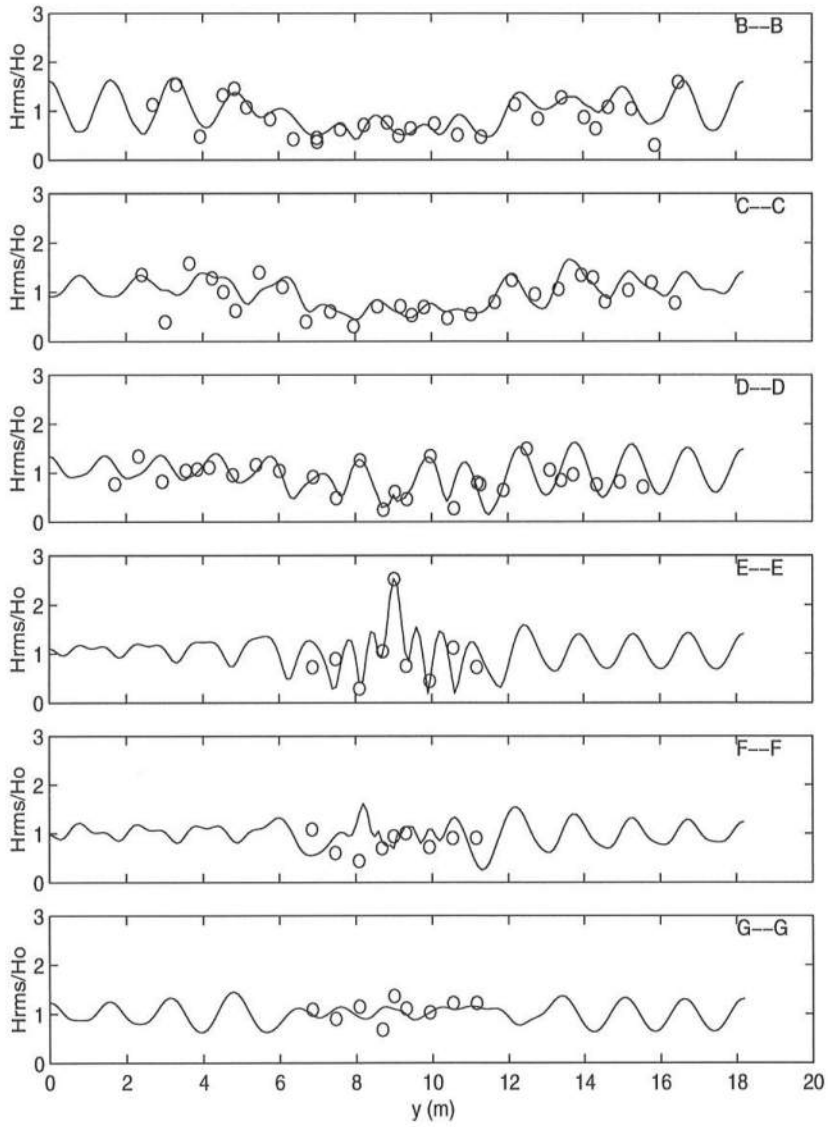

Figure 4: Comparisons of Computed H_{rms} and Chawla and Kirby's (1996) Measurements along Transverse Transects. Solid Lines: Model; Circles: Data. Breaking Waves, Test 4.

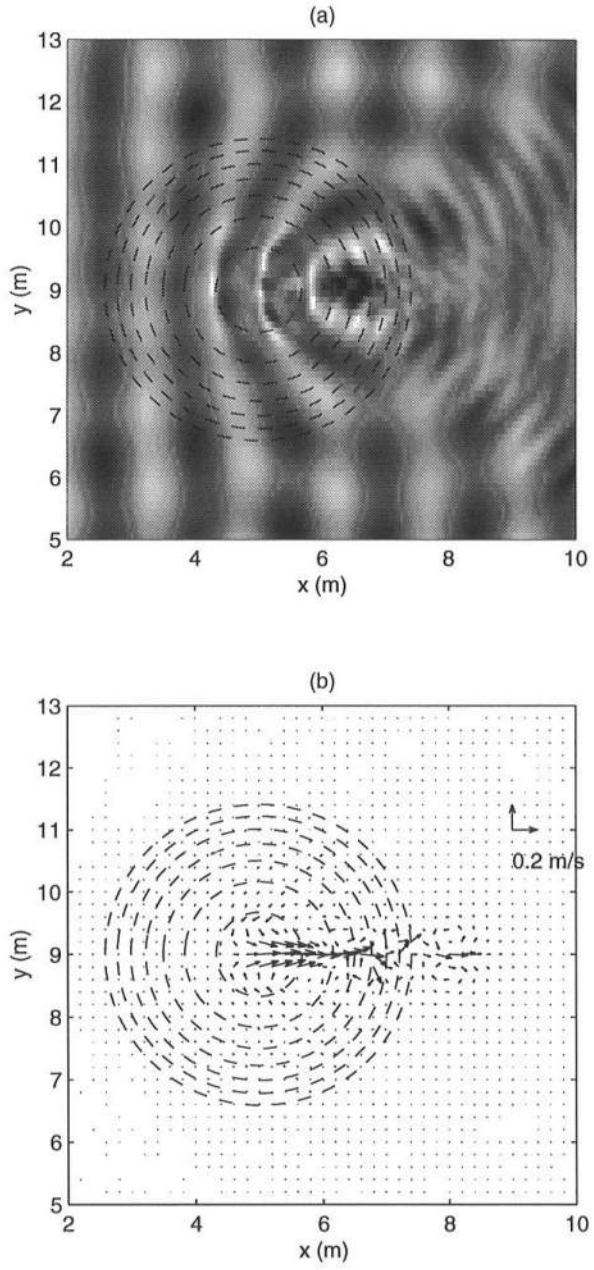

Figure 5: Illustration of (a) Computed Wave Fields and (b) Modelled Underlying Current Field. The Dashed Lines Are the Contours of Water Depth.

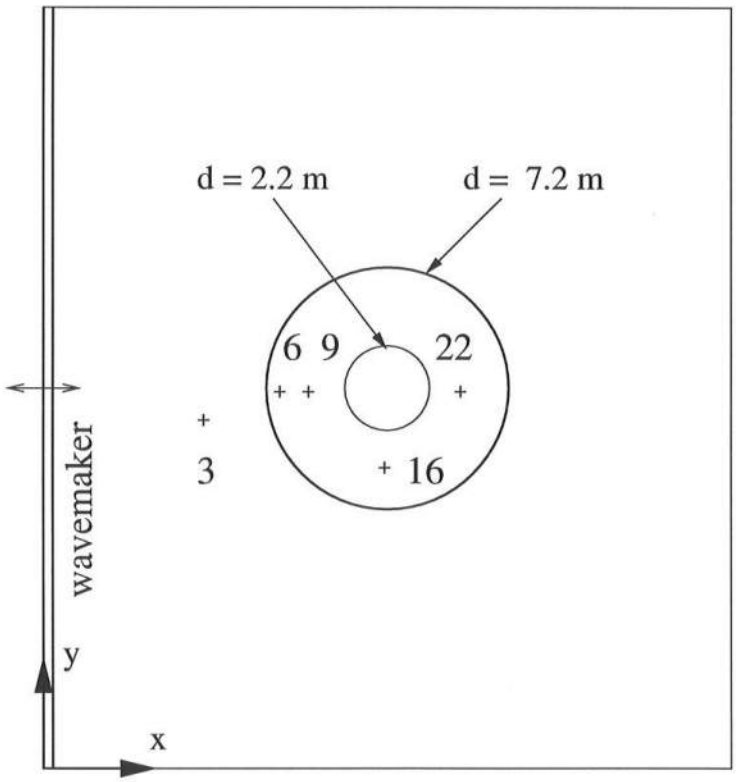

Figure 6: Schematic of the Island and Wave Gauges in Briggs et al.'s (1995) Experiment.

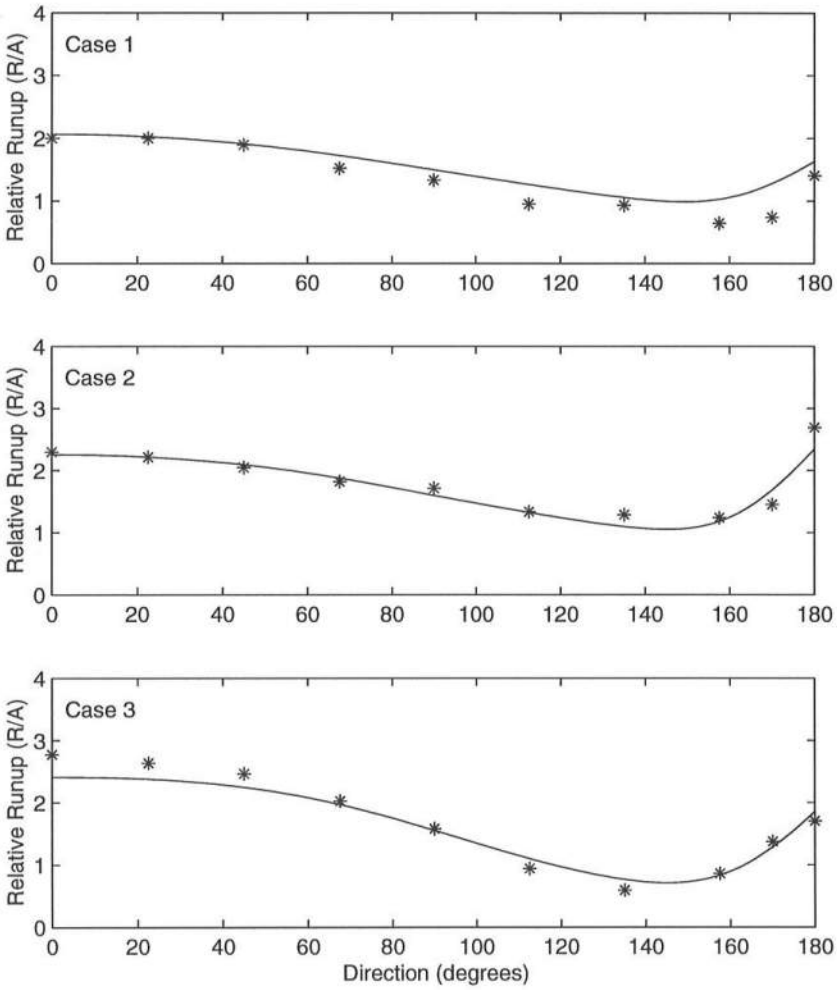

Figure 7: Comparison of Computed and Measured Runup Heights. Stars: Measured; Solid Lines: Computed.

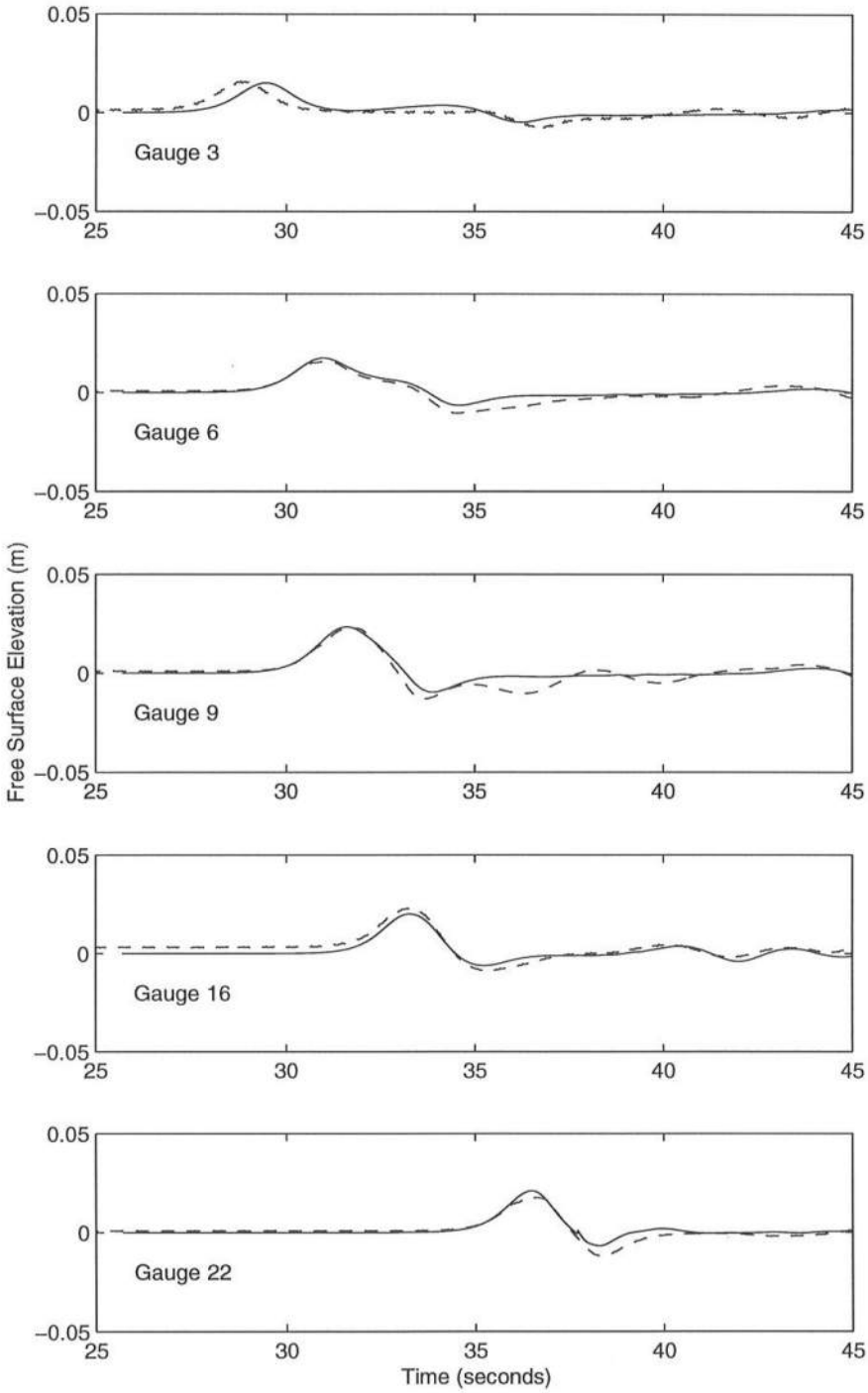

Figure 8: Comparison of Computed and Measured Time Series of Free Surface in Case 1. Dashed Lines: Measured; Solid Lines: Computed.

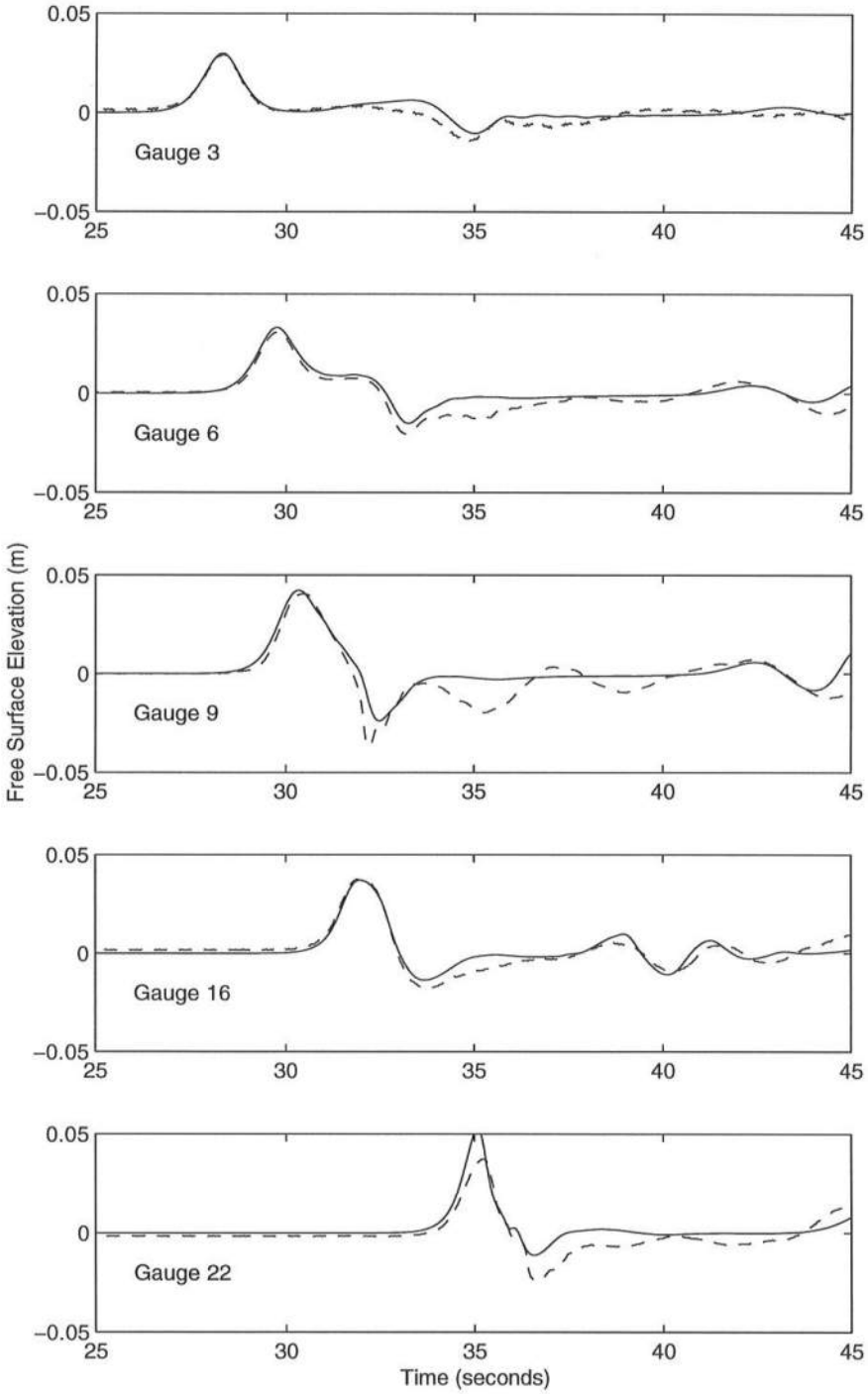

Figure 9: Comparison of Computed and Measured Time Series of Free Surface in Case 2. Dashed Lines: Measured; Solid Lines: Computed.

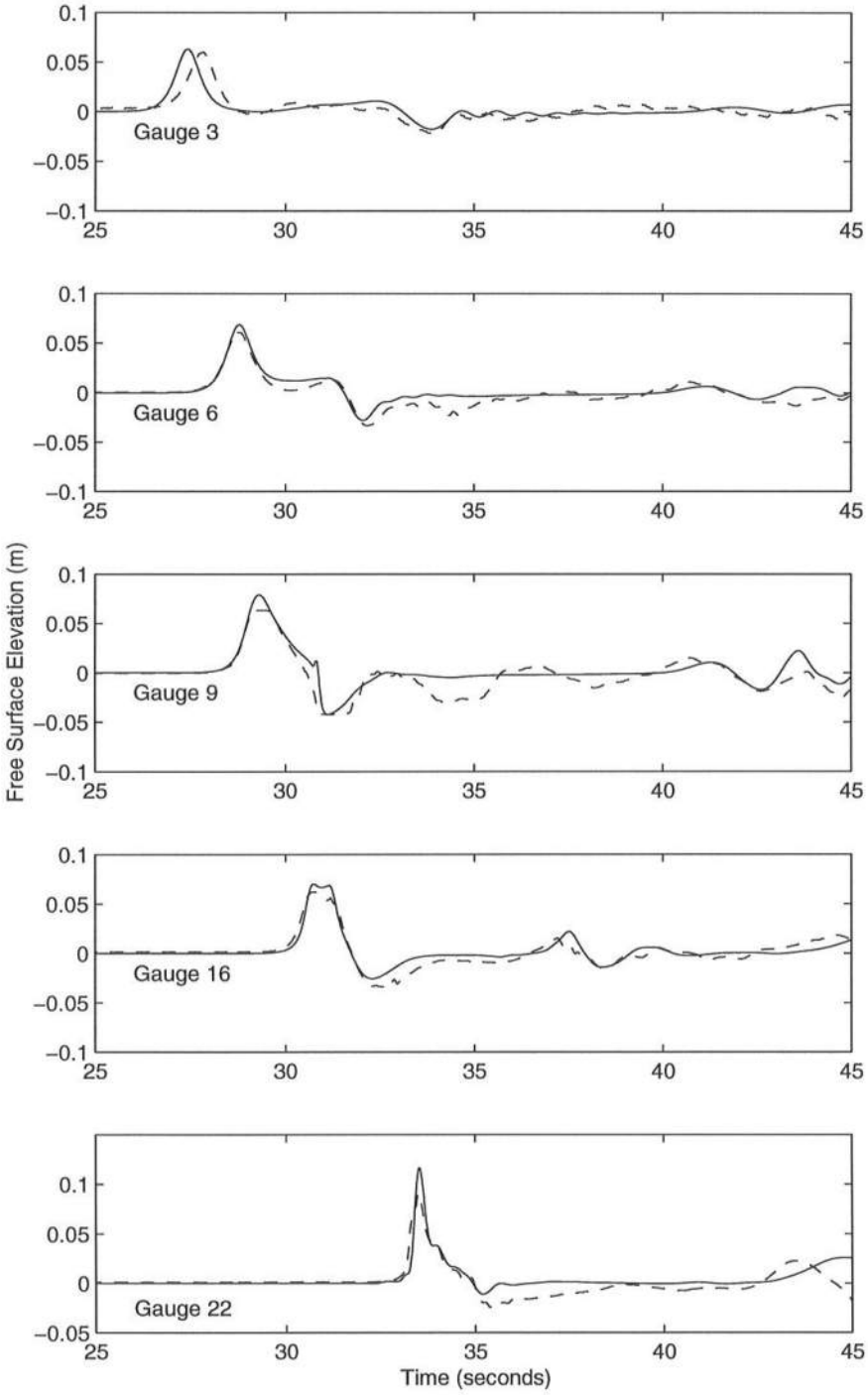

Figure 10: Comparison of Computed and Measured Time Series of Free Surface in Case 3. Dashed Lines: Measured; Solid Lines: Computed.

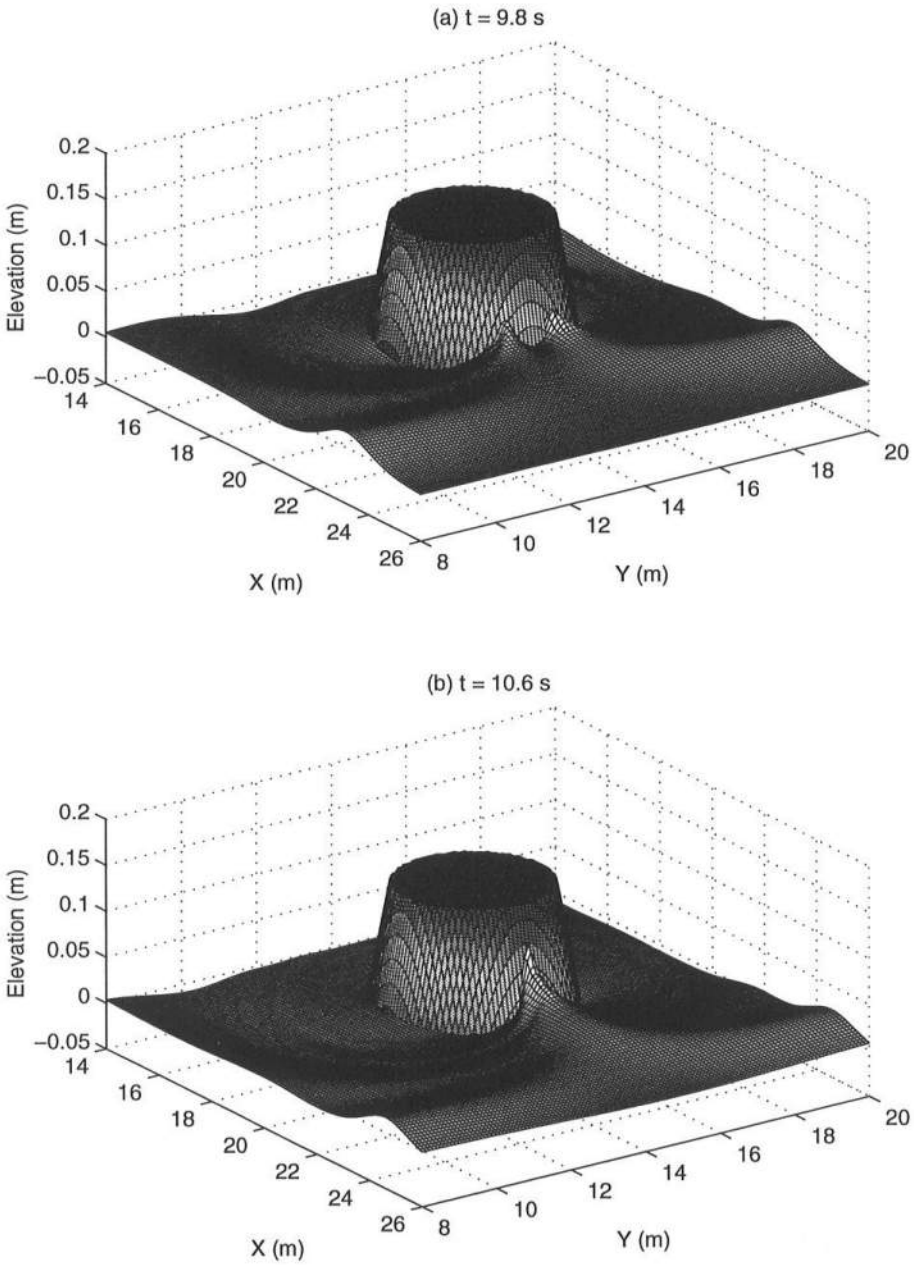

Figure 11: Sequence of Solitary Wave Runup on the Lee Side of the Island in Case 2.

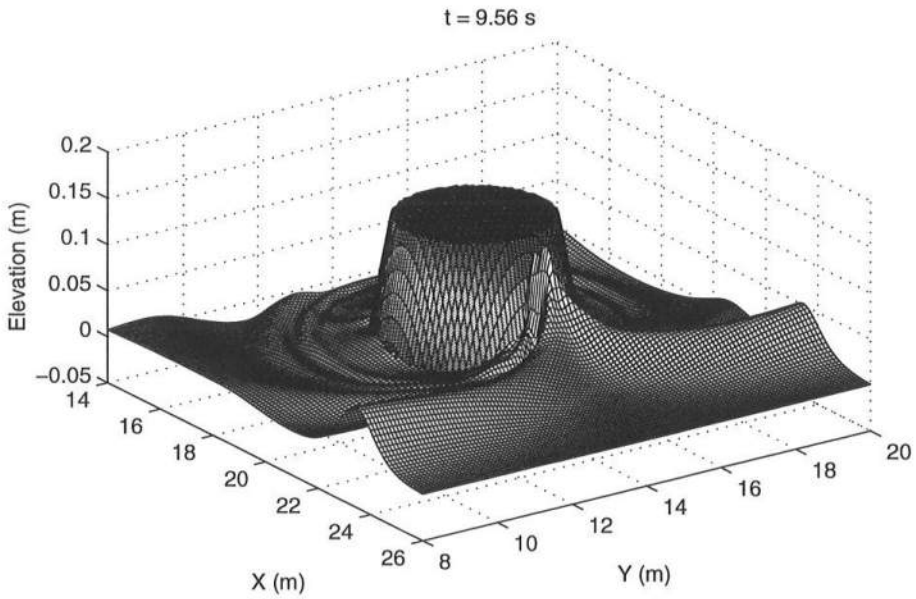

Figure 12: Solitary Wave Runup on the Lee Side of the Island in Case 3.